01/27/2020 version, Brussels, Belgium

Manuscript for Precambrian Research Special issue

"Neoproterozoic Earth-Life System"

(Editor: Frances Westall; Guest editors: Qing Tang, Feifei Zhang)

Primary or secondary? A dichotomy of the strontium isotope anomalies in the Ediacaran strata of Saudi Arabia

Huan Cui[1,2,3,*], Alan J. Kaufman[4], Haibo Zou[5], Fayek H. Kattan[6], Peter Trusler[7], Jeff Smith[7], Andrey Yu. Ivantsov[7,8], Thomas H. Rich[7,9,10], Ashraf Al Qubsani[6], Abdullah Yazedi[6], Xiao-Ming Liu[11], Peter Johnson[12], Steven Goderis[1,2], Philippe Claeys[1,2], Patricia Vickers-Rich[7,8,9,10]

[1] Analytical, Environmental and Geo- Chemistry Group, Division of Earth System Science, Free University of Brussels-VUB, Brussels, Belgium

[2] ET-HOME (Evolution and Tracers of the Habitability of Mars and Earth) Astrobiology Research Consortium, Belgium

[3] State Key Laboratory of Palaeobiology and Stratigraphy, Nanjing Institute of Geology and Palaeontology, Chinese Academy of Sciences, Nanjing 210008, China

[4] Department of Geology and Earth System Science Interdisciplinary Center, University of Maryland, College Park, MD, USA

[5] Department of Geosciences, Auburn University, Auburn, AL 36849, USA

[6] Saudi Geological Survey, Jiddah, Saudi Arabia

[7] School of Earth, Atmosphere & Environment, Monash University, Melbourne, Australia

[8] Paleontological Institute, Russian Academy of Sciences, Moscow, Russia

[9] Palaeontology Department, Museum Victoria, Melbourne, Australia

[10] Department of Chemistry and Biotechnology, Swinburne University of Technology, Melbourne, Australia

[11] Department of Geological Sciences, University of North Carolina, Chapel Hill, USA

[12] 6016 SW Haines Street, Portland, OR 97219, USA

* Corresponding author: huan.cui@vub.be or geohcui@gmail.com (H. Cui)

https://orcid.org/0000-0003-0705-3423 (H. Cui)

Abstract

Secular variation of $^{87}Sr/^{86}Sr$ in sedimentary strata has been widely used in regional and global chemostratigraphic correlations. Typically, diagenesis results in higher $^{87}Sr/^{86}Sr$ signals due to the alteration by Rb-rich fluids and the radiogenic decay of ^{87}Rb to ^{87}Sr. Surprisingly, the $^{87}Sr/^{86}Sr$ values in the Ediacaran limestones from Saudi Arabia (from 0.7029 to 0.7059) are significantly lower than the typical Ediacaran seawater values (mostly from 0.7080 to 0.7090) based on a global compilation. Understanding the origin of these anomalies is important insofar as early macrofossils are preserved in these strata. Two hypotheses have been independently evaluated in this study. The first hypothesis shows a low temperature scenario with isolated oceans or lakes in proximity to a volcanic source. The second hypothesis was characterized by a high temperature scenario with profound overprints by juvenile hydrothermal fluids. Integrated Sr and Nd isotope data reveal that the $^{87}Sr/^{86}Sr$ anomalies are closely coupled with positive $\varepsilon Nd(t=560Ma)$ values (up to +4.1). Based on multiple lines of petrographic, field, and geochemical evidence, the second hypothesis is preferred in this study. We argue that the concept that the Ediacaran biotic radiation took place in an isolated lake environment should be treated with caution. These remarkably low $^{87}Sr/^{86}Sr$ signals have neither temporal nor biogeochemical significance. Sr isotope chemostratigraphy in this particular region may not be a reliable tool for stratigraphic correlations.

Keywords: strontium isotope, neodymium isotope, Ediacaran, early macroorganisms, Saudi Arabia

1. Introduction

The Ediacaran Period (ca. 635–538 Ma) witnessed the initial rise of macroscopic organisms that marks an evolutionary milestone in Earth history before the explosion of Cambrian animals (Narbonne, 2005; Fedonkin et al., 2007; Xiao et al., 2016). However, these early macroscopic organisms, which are most typically preserved as molds and casts in fine-grained siliciclastic rocks, are rare and have wide temporal ranges, which hampers their use as biostratigraphic markers of the Ediacaran time (Knoll, 2000). To solve this problem, strontium isotope ($^{87}Sr/^{86}Sr$) chemostratigraphy has been widely used as a tool for chemostratigraphic correlations of the Precambrian strata due to the long residence time of Sr in the ocean ($\sim10^6$ yrs) and the occurrence of well-preserved marine limestones in many successions (Kaufman et al., 1993; Jacobsen and Kaufman, 1999; Halverson et al., 2007; McArthur et al., 2012). Based on the published $^{87}Sr/^{86}Sr$ data sets worldwide, the range of the Ediacaran seawater $^{87}Sr/^{86}Sr$ compositions is largely between 0.7080 and 0.7090 (Fig. 1) (Halverson et al., 2007; Xiao et al., 2016).

Diagenesis typically increases the $^{87}Sr/^{86}Sr$ signals in the sedimentary record due to the alteration of Rb-rich fluids and the radiogenic decay of ^{87}Rb to ^{87}Sr (Banner, 1995). There are few, if any, clear examples of marine limestones that have become less radiogenic due to diagenetic processes. With this in mind, it is surprising that anomalously non-radiogenic $^{87}Sr/^{86}Sr$ signals (down to 0.7029) were revealed in the Ediacaran carbonate-dominated strata of the Arabian Shield (Miller et al., 2008; Halverson et al., 2013a; Halverson et al., 2013b; this study) (Fig. 2). Insofar as well-preserved Ediacaran limestones worldwide typically have $^{87}Sr/^{86}Sr$ compositions ranging from 0.7080 to 0.7090, the Ediacaran $^{87}Sr/^{86}Sr$ anomalies on the Arabian shield represent a stark enigma that challenges our understanding of the balance between weathering and hydrothermal processes that ultimately control the $^{87}Sr/^{86}Sr$ evolution of the Ediacaran oceans.

Two hypotheses could possibly explain the $^{87}Sr/^{86}Sr$ anomalies in Saudi Arabia. First, these extremely low $^{87}Sr/^{86}Sr$ signals may reflect carbonate deposition in an isolated ocean or lake with $^{87}Sr/^{86}Sr$ values decoupled from the contemporaneous open ocean (Collerson et al., 1988; Ojiambo et al., 2003; Miller et al., 2008; Chesson et al., 2012). The source of these low $^{87}Sr/^{86}Sr$ signals may be from the weathering of local mafic-to-ultramafic hinterland delivered by river runoff during primary sedimentation. If this hypothesis is true, given the preservation of microbial textures and putative Ediacaran macrofossils in the studied sections (Vickers-Rich et al., 2010; Vickers-Rich et al., 2013), it could have profound implications on our understanding of the early evolution of macroorganisms at that time.

Alternatively, given that the mantle is the dominant ^{87}Sr-depleted reservoir on Earth, it is also possible that the $^{87}Sr/^{86}Sr$ anomalies result from significant post-depositional alteration of Ediacaran carbonates by juvenile hydrothermal fluids. However, reports of this scenario in the Ediacaran basins are rare. This hypothesis — though theoretically possible — remains to be fully evaluated for the Ediacaran strata of the Arabian Shield.

This study seeks to elucidate whether the non-radiogenic $^{87}Sr/^{86}Sr$ signals preserved in the Ediacaran carbonates of the Arabian Shield are primary or secondary, and if the latter what unusual geological process was involved. Since mantle-derived neodymium (Nd) isotopes contrast with those of the continental rocks and seawater (White, 2013; Hofmann, 2014) (see section 2 for a detailed explanation), integrated chemostratigraphic, petrographic, and geochemical analyses of a new collection of limestone samples was conducted in order to evaluate these two hypotheses. Our new results reveal complex petrographic features and distinct geochemical values in both strontium and neodymium isotope compositions compared with the Ediacaran backdrop values, which offers important insights to this strontium isotope enigma.

2. Background

2.1. Ediacaran $^{87}Sr/^{86}Sr$ record

Strontium isotope analyses of well-preserved limestone samples from a wide range of Ediacaran basins allow the establishment of a $^{87}Sr/^{86}Sr$ reference curve for the Ediacaran Period. Typically, such a reference profile is supported by stratigraphic correlations based on secular $\delta^{13}C$ trends and radiometric age constraints (Asmeron et al., 1991; Kaufman et al., 1993; Halverson et al., 2007; Macdonald et al., 2013; Bold et al., 2016). Based on an updated $^{87}Sr/^{86}Sr$ compilation (Fig. 1), the Ediacaran $^{87}Sr/^{86}Sr$ trend can largely be divided into four stages:

- In the wake of the Marinoan glaciation, Ediacaran seawater $^{87}Sr/^{86}Sr$ rose rapidly from ~0.7074 to ~0.7080 or even higher (Sawaki et al., 2010; Liu et al., 2013; Liu et al., 2014);
- After the deposition of cap carbonates, the seawater $^{87}Sr/^{86}Sr$ compositions remained ~0.7080 for most of the Ediacaran Period until the next rise during the Shuram $\delta^{13}C$ Excursion (Cui et al., 2015; Cui et al., 2017);
- During the Shuram $\delta^{13}C$ Excursion, seawater $^{87}Sr/^{86}Sr$ compositions rose from ~0.7080 to ~0.7090 (Burns et al., 1994; Calver, 2000; Le Guerroué et al., 2006; Melezhik et al., 2009; Sawaki et al., 2010; Cui et al., 2015);
- During the terminal Ediacaran Period, $^{87}Sr/^{86}Sr$ dropped back to ~0.7080 (Narbonne et al., 1994; Cui et al., 2016a; Cui et al., 2019).

The notable $^{87}Sr/^{86}Sr$ spike within the Marinoan cap carbonates may reflect either global biogeochemical perturbations in the Ediacaran ocean, or simply alteration by late diagenesis. These high $^{87}Sr/^{86}Sr$ values have been interpreted to reflect extreme chemical weathering after the glaciation (Liu et al., 2013; Liu et al., 2014). However, clumped isotope analysis of the Marinoan cap dolostones in South China, which contains similarly high $^{87}Sr/^{86}Sr$ values (Sawaki et al., 2010), suggests the occurrence of significant alteration by hydrothermal fluids (Bristow et al., 2011). Thus, the veracity of the $^{87}Sr/^{86}Sr$ spike in cap carbonates needs further investigation. Regardless, it is obvious that the seawater $^{87}Sr/^{86}Sr$ values in most of the Ediacaran Period range between 0.7080 and 0.7090. Therefore, the extremely low $^{87}Sr/^{86}Sr$ values (0.7029 to 0.7059) measured from the Ediacaran carbonates in the Arabian Shield represent a profound isotopic anomaly (Fig. 2) and warrant further investigations.

2.2. Sr–Nd isotope system

In this study, an approach of integrated Sr–Nd isotope analyses was used to evaluate the different origins (i.e., primary or secondary) of the $^{87}Sr/^{86}Sr$ anomalies in the Ediacaran carbonates of the Arabian Shield. Sr and Nd cycles in the seawater have very different behaviors in the modern oceans. The average Sr concentration of the modern surface ocean water is 87.40 μMol/kg (±0.56%) (de Villiers, 1999). The main input of Sr in the ocean is from chemical weathering of the continental crust and, in a lesser amount, hydrothermal flux from the mid-ocean ridges (McArthur et al., 2012). Given the much longer residence time of Sr (~10^6 years) in the ocean than seawater mixing time (~1500 years), Sr is homogenous in modern oceans (Broecker and Peng, 1982; Broecker, 2003; Kuznetsov et al., 2012).

In contrast with the very soluble Sr in the seawater, Nd is highly insoluble. Nd concentration in seawater is very low, which generally ranges ~15–45 pMol/kg (Note: pMol/kg = 10^{-12}Mol/kg) (Goldstein and Hemming, 2014). Therefore its isotopic composition in seawater is very heterogeneous given the very short residence time in the oceans (360 to 700 years, shorter than the mean ocean mixing time) (Taylor and McLennan, 1985; Alibo and Nozaki, 1999; Tachikawa et al., 2003; Lacan et al., 2012; Rudnick and Gao, 2014; Tachikawa et al., 2017).

By convention, $^{143}Nd/^{144}Nd$ ratios are often reported relative to the Chondritic Uniform Reservoir (CHUR) using the ε notation, which represent the relative deviation of the $^{143}Nd/^{144}Nd$ ratio from the chondritic ratio in 10,000. ^{143}Nd is the product of the radiogenic decay of ^{147}Sm. Both Nd and Sm are rare earth elements (REEs), but Nd is more incompatible than Sm and is therefore more enriched in the crust than in the mantle during mantle-crust differentiation (Hofmann, 2014). Consequently the crust with lower Sm/Nd ratio typically results in negative εNd values, and conversely, the depleted mantle with higher Sm/Nd ratio typically results in positive εNd values (Jacobsen and Wasserburg, 1980; White, 2013).

Based on the Sr–Nd isotope system, the geochemical source of the samples can be predicted. If the samples preserve negative εNd composition, continental crust signals should dominate the composition of the samples. Alternatively, if the samples preserve positive εNd values, significant amount of mantle-derived juvenile signals should have been registered.

3. Geological settings

The youngest sequence in the Ediacaran basins of the studied region is the Jibalah Group. This group was originally defined by Delfour (1970) and extended to include other formations of volcanic and sedimentary rocks that are separately named in various parts of the Shield (Johnson, 2006). For example, the Saluwah, Sulaysiyah, Naghr, Misyal, Salih, Mataar, Dhaiqa and Muraykah formations in the northwest, and the Zarghac and Jifn formations in the north (Johnson, 2006). These formations have all been included to the Jibalah Group due to the non-metamorphosed preservation and their inferred Ediacaran age. Typically, the outcrops of the Jibalah Group are red, brown, or purplish sandstones, conglomerates, and stromatolitic limestones (Figs. 5–7). This group has been regarded to be equivalent to the Ediacaran Nafun Group (ca. 635–547 Ma) in Oman (Allen, 2007).

The two studied sections are the Naghr Formation and the Dhaiqa Formation in the NW Arabian Shield (Figs. 3–5). The Naghr formation is composed of sandstones with horizons of conglomerate and lesser amounts of siltstone and limestones (containing stromatolitic textures) (Vickers-Rich et al., 2010; Vickers-Rich et al., 2013). Multiple conglomerate intervals have also been found in the studied sections. In this region, the Cambrian Siq sandstones overlie the Neoproterozoic Jibalah Group, forming a sharp unconformity (Fig. 4) (Miller et al., 2008; Vickers-Rich et al., 2013). Notably, late Cenozoic flooding basalts cover large areas of the Arabian Shield (Fig. 6D) (Camp and Roobol, 1989; Henjes-Kunst et al., 1990). Basalt intrusions are superimposed in multiple stages with time ranging from ~1 Ma to ~30 Ma (Moufti et al., 2012).

Geochronologic constraints suggest that the Dhaiqa Formation is mid- to late Ediacaran. The Dhaiqa Formation, together with the underlying Maatar Formation, are exposed in an isolated sedimentary basin unconformable on both the Bayda Group and the Marabit-suite granite, which implies that they are younger than 620 Ma (Johnson, 2006). The U–Pb age constraint measured by LA-ICP-MS of detrital zircons in the Dhaiqa Formation reveals the youngest detrital age of 569 ±

3.0 Ma, suggesting a maximum depositional age in the middle-late Ediacaran Period (Vickers-Rich et al., 2010; Vickers-Rich et al., 2013). The U–Pb ages of 599 ± 4.8 Ma and 570 ± 4.6 Ma analyzed in the core and rim of the youngest detrital zircon, respectively, from a diamictite bed in the middle Dhaiqa Formation also suggest an Ediacaran depositional age (Miller et al., 2008).

Members of the Ediacara-type macrofossils *Beltanelliformis* and *Harlaniella* were found in the studied sections (Figs. 8–10) (Vickers-Rich et al., 2010; Vickers-Rich et al., 2013; Ivantsov et al., 2014b). The macrofossils, *Beltanelliformis minutae* McIlroy, Crimes, Pauley, 2005 and *Beltanelliformis* sp. were found in the Naghr and Muraykha formations (Figs. 8A–C, 10E), which have been interpreted as large spherical colonies of cyanobacteria (Ivantsov et al., 2014a; Ivantsov et al., 2014b). It is worth mentioning that a more recent biomarker study has confirmed the cyanobacteria origin of *Beltanelliformis* (Bobrovskiy et al., 2018). Tubular fossil *Harlaniella ingriana* Ivantsov, 2013 were found in the Dhaiqa and Muraykhah formations (Figs. 9A, 9F, 9G, 10D), which have been interpreted as internal casts and impressions of fragments of tubes of initially organic composition (Ivantsov, 2013; Ivantsov et al., 2014b). In addition, some specimens in frond-like forms have also been found directly under volcanic ash layers (Fig. 9C, 9D), which look similar to the iconic Ediacara-type fossil *Charniodiscus,* though detailed features are lacking. Also, ripple marks (Figs. 8D, 9B), microbially-induced "elephant skin" structures (Fig. 8E) and *Arumberia* (Fig. 8F) were found in the studied sections, suggesting shallow environments.

4. Geochemical methods

The geochemical analyses in this study include paired carbonate carbon ($\delta^{13}C_{carb}$) and oxygen ($\delta^{18}O_{carb}$) isotopes, organic carbon isotopes ($\delta^{13}C_{org}$), total organic carbon content (TOC), Sr isotopes ($^{87}Sr/^{86}Sr$), Nd isotopes (εNd), and concentrations of major and trace elements.

All the isotopic analyses were conducted in the Department of Geology, University of Maryland. Elemental concentrations were analyzed in the Carnegie Institution of Washington. Detailed methods have been published in previous papers (Puchtel et al., 2013; Cui et al., 2015; Cui et al., 2016a; Cui et al., 2016b; Liu et al., 2016). Here we briefly summarize them as below.

4.1. Major and trace elemental analysis

Major and trace elemental abundances of micro-drilled carbonates were analyzed for a few representative samples in order to better evaluate the degree of diagenetic alteration. Aliquots of the micro-drilled carbonate powders were dissolved in 0.4 M HNO_3, centrifuged, and only analyzed for the solutions. Any clays, if present, would not have been dissolved by the dilute acid. The resulting solutions were analyzed on a Thermo Scientific® iCAP-Q ICP-MS (Inductively Coupled Plasma – Mass Spectrometry) at the Carnegie Institution of Washington. Precision of these analyses as determined by repeated measurements of a house standard carbonate was < 5% (2σ) for major elements and < 10% (2σ) for trace elements and REEs.

4.2. Sr and Nd isotope analyses

Sr and Nd isotopes were analyzed on a VG Sector 54 and ThermoFisher Triton Multicollector Thermal Ionization Mass Spectrometers (TIMS), respectively, in the University of Maryland TIMS Lab. Given the very different concentration of Sr and Nd in carbonates, around 10 mg and 100 mg finely crushed powder were dissolved for Sr and Nd isotope analyses, respectively. In order to only digest the carbonate portion and avoid the contamination of silicate minerals, we used 0.5 M acetic acid (for Sr) and 0.5 M nitric acid (for Nd) to dissolve the studied limestone samples. Final Sr isotope data have been corrected for fractionation using the standard value $^{86}Sr/^{88}Sr = 0.1194$. Repeated analysis of the NBS SRM987 standard during Sr isotope analysis yielded an average value of $^{87}Sr/^{86}Sr = 0.710245 \pm 0.000011$ (2σ). Detailed method of Sr isotope analysis can be found in our previous published papers (Cui et al., 2015; Cui et al., 2016a; Cui et al., 2017).

For Nd isotope analysis, the REE were first separated from the silicate matrix using HCl cation exchange chromatography, and then the Nd fraction was separated and purified using 2-methyllactic acid cation exchange chromatography. The effects of mass-fractionation were corrected for using an exponential law via normalizing to $^{146}Nd/^{144}Nd = 0.7219$. The $^{143}Nd/^{144}Nd$ value for a 300 ng load of the AMES standard run during the analytical campaign was 0.512154 ± 5 (2SE). The additional analytical details are provided in Puchtel et al. (2013).

The initial εNd(0) values were calculated on the basis of the present-day parameters of the chondrite uniform reservoir (CHUR). The calculated εNd(t) values are based on the assumption of a depositional age t=560 Ma, which is the best available age constraint thus far for the studied sections.

$$^{147}Sm/^{144}Nd(0)_{sample} = ([Sm]/A_{Sm} \times [^{147}Sm_{natural}])/([Nd]/A_{Nd} \times [^{144}Nd_{natural}]) = (Sm/Nd)/1.654 \quad (1)$$

$$^{143}Nd/^{144}Nd(t)_{sample} = {}^{143}Nd/^{144}Nd(0)_{sample} - {}^{147}Sm/^{144}Nd(0)_{sample} \times (e^{\lambda t} - 1) \quad (2)$$

$$^{143}Nd/^{144}Nd(t)_{CHUR} = {}^{143}Nd/^{144}Nd(0)_{CHUR} - {}^{147}Sm/^{144}Nd(0)_{CHUR} \times (e^{\lambda t} - 1) \quad (3)$$

$$\varepsilon Nd(t) = [^{143}Nd/^{144}Nd(t)_{sample}/^{143}Nd/^{144}Nd(t)_{CHUR} - 1] \times 10{,}000 \quad (4)$$

The Sm and Nd concentration data used for the calculation of $^{147}Sm/^{144}Nd(0)_{sample}$ (Eq. 1) were analyzed from separate aliquots in Carnegie Institution of Washington (see section 4.1). The parameter t in Eqs. 2–4 represents the age (ca. 560 Ma) of the samples in this study. The natural abundances of ^{147}Sm and ^{144}Nd are $^{147}Sm_{natural}$ = 0.1499, $^{144}Nd_{natural}$ = 0.23798, respectively (Berglund and Wieser, 2011). The atomic weights of Sm and Nd are A_{Sm} = 150.36, A_{Nd} = 144.242, respectively (Meija et al., 2016). The decay constant (λ) of ^{147}Sm is 6.54×10^{-12} yr^{-1} (Lugmair and Marti, 1978). The present-day parameters of the chondrite uniform reservoir (CHUR) are $^{147}Sm/^{144}Nd$ = 0.1967 (Jacobsen and Wasserburg, 1980) and $^{143}Nd/^{144}Nd$ = 0.512638 (Hamilton et al., 1983).

4.3. Carbonate C and O isotope analysis

Powders for $\delta^{13}C_{carb}$ and $\delta^{18}O_{carb}$ analyses were collected on polished slabs using a press micro-drill. Micro-drilling was guided by petrographic fabrics so that the best-preserved zones were sampled for further geochemical measurement. We indeed found a few horizons with heavily recrystallized carbonate or veins, but those were strictly avoided during sampling. The precision for both carbon and oxygen isotopes based on repeated measurement of reference materials was routinely better than 0.1‰.

4.4. Organic C isotope analysis

The $\delta^{13}C_{org}$ compositions of bulk powders were measured by combustion of decalcified residues to CO_2 with a Eurovector elemental analyzer in-line with an Elementar Isoprime isotope ratio mass spectrometer. Approximately 15 grams of core chips lacking secondary veins or weathered surfaces were crushed and repeatedly (2× or more) acidified with 3 M HCl overnight to quantitatively remove carbonate. These residues were then washed with ultra-pure Milli-Q water to neutral pH, decanted, and dried in an 80°C oven overnight for subsequent $\delta^{13}C_{org}$ analysis. Uncertainties for $\delta^{13}C_{org}$ measurements determined by multiple analyses of standard materials were better than 0.1‰. Detailed method can be found in our previous published papers (Cui et al., 2015; Cui et al., 2016a; Cui et al., 2017).

4.5. Micro X-Ray Fluorescence

High-resolution elemental abundance maps of the polished sample surfaces were produced using the Tornado M4 micro X-Ray Fluorescence (µXRF) scanner (Bruker nano GmbH, Berlin, Germany) at the Vrije Universiteit Brussel, Belgium. µXRF mapping was performed along a 2D grid with 25 µm spacing, a spot size of 25 µm and an integration time of 1 ms per pixel. The X-Ray source was operated under maximum energy settings (600 µA, 50 kV) with no source filters. This mapping approach by µXRF resulted in qualitative element concentration distributions on the elemental maps.

5. Results

5.1. Petrographic results

Petrographic observations of the studied samples show significant heterogeneity in textures (Figs. 11–13). Many samples exhibit strong recrystallization under polarized light. Interbedded carbonate-rich and siliciclastic-rich laminae are also abundant (Figs. 11A–B, 12A–B, 12I–H).

5.2. Geochemical results

In total 14 samples were selected for $^{87}Sr/^{86}Sr$ analysis in this study. The $^{87}Sr/^{86}Sr$ values measured from the carbonate portion range from 0.7029 to 0.7059, which are all significantly lower than the typical Ediacaran seawater values (mostly from 0.7080 to 0.7090) (Figs. 1, 2). Among the samples for $^{87}Sr/^{86}Sr$ analyses, 5 samples were selected for Nd isotope analyses, and yield positive εNd(t=560Ma) values (Fig. 12), in strong contrast with the negative εNd(t) values analyzed from other Ediacaran sedimentary samples worldwide (Figs. 17, 18). It is worth noting that Sr-Nd isotopic compositions of our 5 samples display a negative correlation (Fig. 15F).

Trace element data show that the samples are mostly rich in Sr (concentration data ranging from 84.2 ppm up to 815.5 ppm). The Rb concentration data range from 0.2 ppm to 16.2 ppm in the studied samples.

The $\delta^{13}C_{carb}$ compositions of micro-drilled powder range from –3.8‰ to 6.0‰, with an average value of 2.1‰ in the samples. The $\delta^{18}O_{carb}$ compositions of the micro-drilled samples range from 1.8‰ to –13.7‰, with an average value of –9.1‰. The $\delta^{13}C_{org}$ compositions of acidified residuals range from –17.1‰ to –32.1‰, with an average value of –27.5‰. All the data can be found in the supplementary material.

6. Discussion

6.1. $\delta^{13}C_{carb}$ chemostratigraphy

A global comparison between the $\delta^{13}C_{carb}$ profile of the Dhaiqa Formation and the published profiles of other mid- to late Ediacaran sections reveals both similarities and differences. The $\delta^{13}C_{carb}$ profile of the Dhaiqa Formation shows scattered but overall positive values (Fig. 16A), in contrast with the published $\delta^{13}C_{carb}$ profile of the roughly equivalent Muraykhah Formation of the Jibalah Group in the Antaq basin, where an overall increasing trend with mostly negative $\delta^{13}C_{carb}$ values was recorded (Nettle et al., 2014) (Fig. 16B). It is likely that the analyzed Muraykhah section (Fig. 16B) captured the recovering part of the Shuram Excursion, therefore is slightly older than the Dhaiqa section that captured mostly post-Shuram values (Fig. 16A).

The lack of a clear trend in the analyzed Dhaiqa Formation prohibits detailed stratigraphic correlation with other Ediacaran sections. Regardless, the overall positive $\delta^{13}C_{carb}$ values are consistent with the late Ediacaran backdrop $\delta^{13}C_{carb}$ values from other basins, which typically show positive values after the Shuram excursion (Fig. 16C–E).

6.2. Evaluating the isolated lake hypothesis

Could the coupled Sr–Nd anomalies in Saudi Arabia result from an isolated ocean or lake during the Ediacaran Period? Published studies reveal that modern river waters and seawaters are typically dominated by weathered continental crust materials with negative εNd values (Goldstein et al., 1984; Goldstein and Jacobsen, 1987; Tachikawa et al., 2017). However, in very rare cases, river waters with positive εNd values (up to +8) have also been found (Goldstein and Jacobsen, 1987; Allègre et al., 2010), which reflects a predominantly young volcanic source (Rad et al., 2007; Allègre et al., 2010). In the modern ocean, the highest εNd value of +2.7 is found in the Eastern Equatorial Pacific where young volcanogenic material is abundant (Grasse et al., 2012).

With the above in mind, to form primary carbonates with anomalously low $^{87}Sr/^{86}Sr$ and exceptionally positive εNd signals, three conditions should be met. First, the water mass has to be isolated and stagnant in order to decouple the depositional environment from the Ediacaran open ocean; Second, the depositional environment should be in close proximity to juvenile sources (e.g., island arcs) in order to capture the juvenile Sr–Nd signals during deposition; Third, such rare paleogeographic conditions should be maintained on a prolonged geological time scale (i.e., millions of years) so that the $^{87}Sr/^{86}Sr$ anomalies can be preserved in carbonates or calcareous sandstones for hundreds of meters in thickness in the Arabian Shield (Fig. 4, 5).

Theoretically, the above scenario could have possibly existed if all the three conditions were met at the same time. Geological evidence indeed indicates that the depositional environments of the studied sections were not typical marine platforms. First, both sections show significant input of siliciclastic components during deposition. Interbedded siliciclastics, calcareous sandstones, conglomerates are not uncommon in the studied sections. Many carbonates are rich in siliciclastic grains with low textural maturity (i.e., angular grain shapes) (Fig. 13A–F), suggesting a deposition environment in proximity to the weathered source. That being said, it is also notable that most of the grains in carbonate samples are quartz (Fig. 13A–J). No mafic or ultramafic detrital grains have been found in the studied samples.

Second, published studies show that magmatism was active during the Cryogenian and Ediacaran periods (Johnson et al., 2011; Johnson, 2014). Multiple igneous intrusions in the Arabian Shield have been dated and the results reveal Cryogenian and Ediacaran ages (Kozdrój et al., 2018) (Fig. 3C). Therefore, it is possible that igneous activities at that time produced a considerable amount of juvenile materials, which were subsequently weathered into restricted oceans nearby.

In summary, although the possibility of carbonate precipitation in an isolated ocean in close proximity to an Ediacaran juvenile source is not very likely, we have not completely ruled out this hypothesis. Supporting evidence for this hypothesis is not sufficient at the moment. It remains open for further testing.

6.3. Evaluating the juvenile hydrothermal fluid hypothesis

In parallel with the "low temperature scenario" characterized by an isolated ocean (section 6.2), a "high temperature scenario" with basin-scale alteration by juvenile hydrothermal fluids can also possibly account for the anomalous Sr–Nd signals in this study. Multiple lines of evidence suggest that the $^{87}Sr/^{86}Sr$ anomaly may be post-depositional in origin. First, petrographic observation shows abundant veins (Fig. 12K–N) and highly recrystallized carbonate fenestrae (Figs. 12C, 12D, 13K, 13L) or laminae (Figs. 12G–J, 13G–J), indicating the occurrence of hydrothermal alteration by external fluids. Second, considering that no positive εNd signals up to +4 have been found in open ocean seawaters or modern marine carbonates, it is more likely that the positive εNd(t=560Ma) signals preserved in the Ediacaran limestones in this study resulted from juvenile hydrothermal fluids.

Supporting evidence for a hydrothermal origin of the Sr–Nd anomalies also comes from the field. In addition to the Cryogenian and Ediacaran intrusions (Johnson et al., 2011; Johnson, 2014; Kozdrój et al., 2018) (Fig. 3C), late Cenozoic flooding basalts cover large areas of the Arabian Shield (Fig. 6D) (Miller et al., 2008; Moufti et al., 2012; Vickers-Rich et al., 2013). It is possible that during the Ediacaran magmatic activities or the Cenozoic flood basalt event on the Arabian Shield, a considerable amount of juvenile hydrothermal fluids migrated upwards, percolated the Ediacaran carbonate successions, and reset the Sr–Nd isotopic compositions. Published studies show that the Ediacaran granites in the Arabian Shield and adjacent parts of the Sinai Peninsula to the north have positive εNd values of +1.1 to +5.4 and initial $^{87}Sr/^{86}Sr$ values of 0.6194–0.7053 (Be'eri-Shlevin et al., 2010; Moghazi et al., 2012; Robinson et al., 2015), and those younger than ~600 Ma have been modeled as emplaced in extensional, within-plate and back-arc settings associated with lithospheric delamination and slab-break-off, with magma derived from an enriched MORB-type mantle wedge subjected to crustal assimilation and fractionation (Moghazi et al., 2012; Robinson et al., 2015). In addition, Miocene dikes and granites emplaced along the Red Sea margin of the

Arabian Peninsula have initial $^{87}Sr/^{86}Sr$ values of 0.7043–0.7063 (Baldridge et al., 1991; Coleman et al., 1992), which can all be the sources of juvenile hydrothermal fluids.

Taken together, we propose that it is more likely that the $^{87}Sr/^{86}Sr$ anomalies in this region resulted from profound overprints by juvenile hydrothermal fluids. This interpretation is consistent with independent sedimentological observations that most of the samples have been clearly recrystallized and are associated with basalt intrusions in this region.

6.4. Implications for early metazoan evolution

Our new data also shed light on the biogeochemical reconstruction of the Ediacaran ocean in the Saudi Arabian Shield region, which harbors some of the earliest macroorganisms in Earth history. Based on the anomalous low $^{87}Sr/^{86}Sr$ data, it has been speculated that animal evolution during the Ediacaran Period in this region may be associated with anomalous environments, possibly an isolated lake (Miller et al., 2008). Similar speculation has also been proposed based on a study of clay minerals from the fossiliferous Doushantuo Formation of South China (Bristow et al., 2009; see also Huang et al., 2013 for a re-interpretation). If these hypotheses are true, the earliest animal life may evolve from locally restricted lake environments, instead of marine environments.

However, based on the new petrographic and geochemical results in this study, we argue that it is more likely that the $^{87}Sr/^{86}Sr$ anomalies in the northern Arabian Shield represent profound overprints by juvenile hydrothermal fluids, and therefore cannot be used for biogeochemical reconstructions of the paleoenvironment that hosted the Ediacaran biota in this region. Sr isotope chemostratigraphic correlations in this region should be made with caution.

7. Conclusions

In this study, detailed petrographic and geochemical analyses were conducted for the Ediacaran limestone and calcareous sandstone samples from the Arabian Shield. Integrated Sr and Nd isotope data reveal that the $^{87}Sr/^{86}Sr$ anomalies (from 0.7029 to 0.7059) are closely coupled with positive εNd(t=560Ma) values (up to +4.1).

Two hypotheses have been independently evaluated based on the current results. The first hypothesis shows a low temperature scenario with isolated oceans or lakes in proximity to a mafic to ultramafic source. The second hypothesis was characterized by a high temperature scenario with profound overprints by juvenile hydrothermal fluids. Based on integrated petrographic, field, and geochemical data, the second hypothesis is preferred in this study.

If the second hypothesis is true, the concept that the Ediacaran biotic radiation took place in an isolated lake environment should be treated with caution; Sr isotope chemostratigraphy in this region may not be a reliable tool for stratigraphic correlations.

Acknowledgements

This paper is a contribution to the Precambrian Research special collection "Neoproterozoic Earth-Life System". We would like to thank Igor Puchtel and Valentina Puchtel for their guide in Nd isotope analysis; the Saudi Geological Survey for their support, especially Naser Jahdali, for his assistance in the field; Xin-Yuan Zheng for helpful discussion. This paper was improved by constructive reviews by XXX and XXX. We thank XXX (editor) and XXX (guest editor) for handling this manuscript.

This study was supported by funding from the Australian International Geoscience Program (IGCP) Committee, the UNESCO IGCP Board for project IGCP587, and the National

Geographic Society grant to PVR. Geochemical analyses in UMD was funded by the Geological Society of America (GSA) graduate student research grant to HC. HC also want to acknowledge the open research grant from the State Key Laboratory of Palaeobiology and Stratigraphy, Nanjing Institute of Geology and Palaeontology, Chinese Academy of Sciences.

Figure and captions

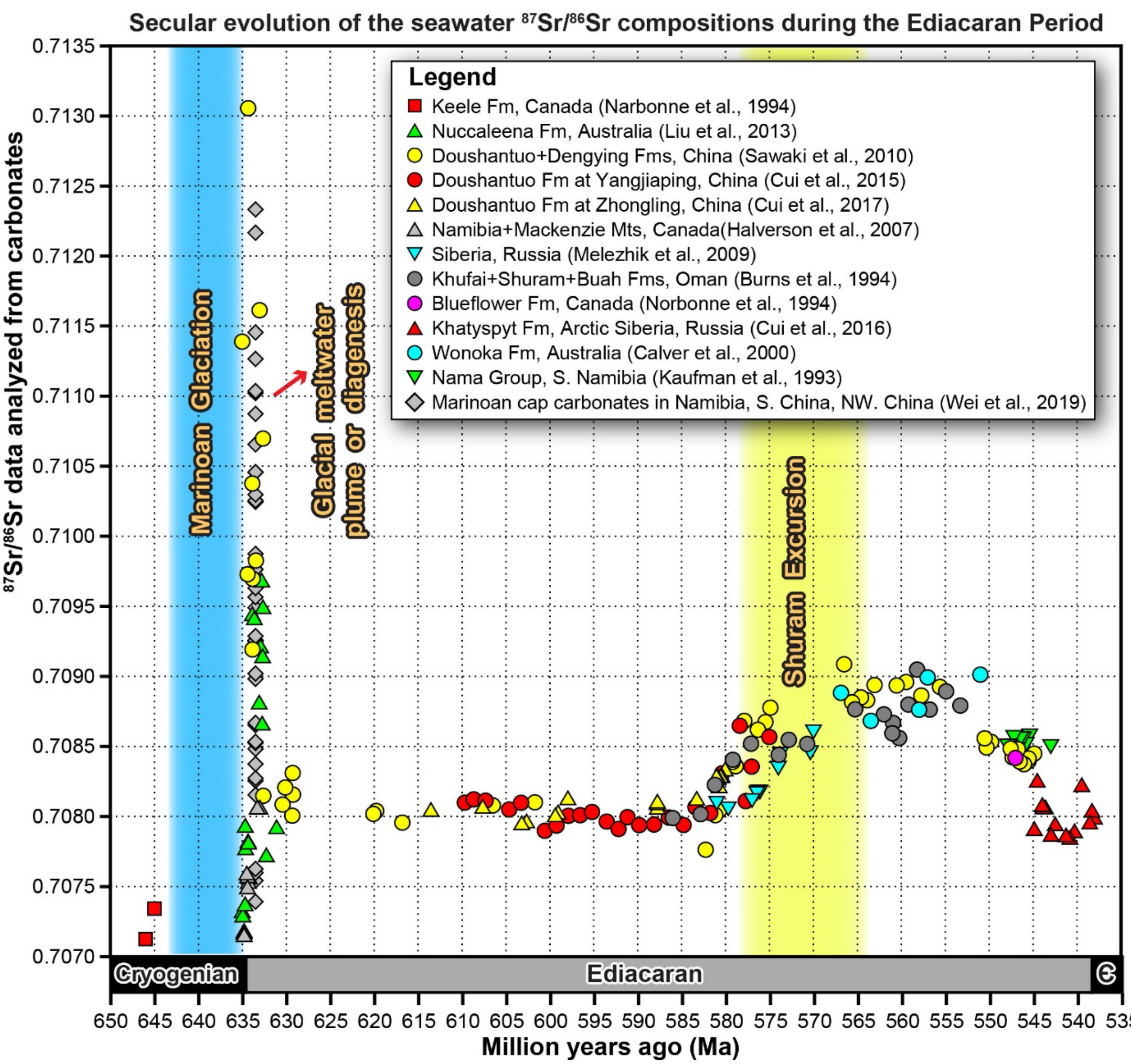

Figure 1. Time-series $^{87}Sr/^{86}Sr$ profile of the Ediacaran Period (ca. 635–538 Ma). Data source: Keele Formation, Canada (Narbonne et al., 1994); Nuccaleena Formation, Australia (Liu et al., 2013); Doushantuo and Dengying formations in the Three Gorges area, South China (Sawaki et al., 2010); Doushantuo Formation at Yangjiaping (Cui et al., 2015); Doushantuo Formation at Zhongling (Cui et al., 2017); Ediacaran strata in Siberia, Russia (Melezhik et al., 2009); Khufai, Shuram, and Buah formations in Oman (Burns et al., 1994); Blueflower Formation, Canada (Narbonne et al., 1994); Khatyspyt Formation in Arctic Siberia, Russia (Cui et al., 2016a); Wonoka Formation, Australia (Calver, 2000); Nama Group, southern Namibia (Kaufman et al., 1993); Maieberg Formation, northern Namibia and Hayhook Formation of the Mackenzie Mountains, Canada (Halverson et al., 2005; Halverson et al., 2007); Marinoan cap carbonates in Keilberg Member of Nanibia, Doushantuo Formation of South China, and the Sugetbrak Formation of NW China (Wei et al., 2019a).

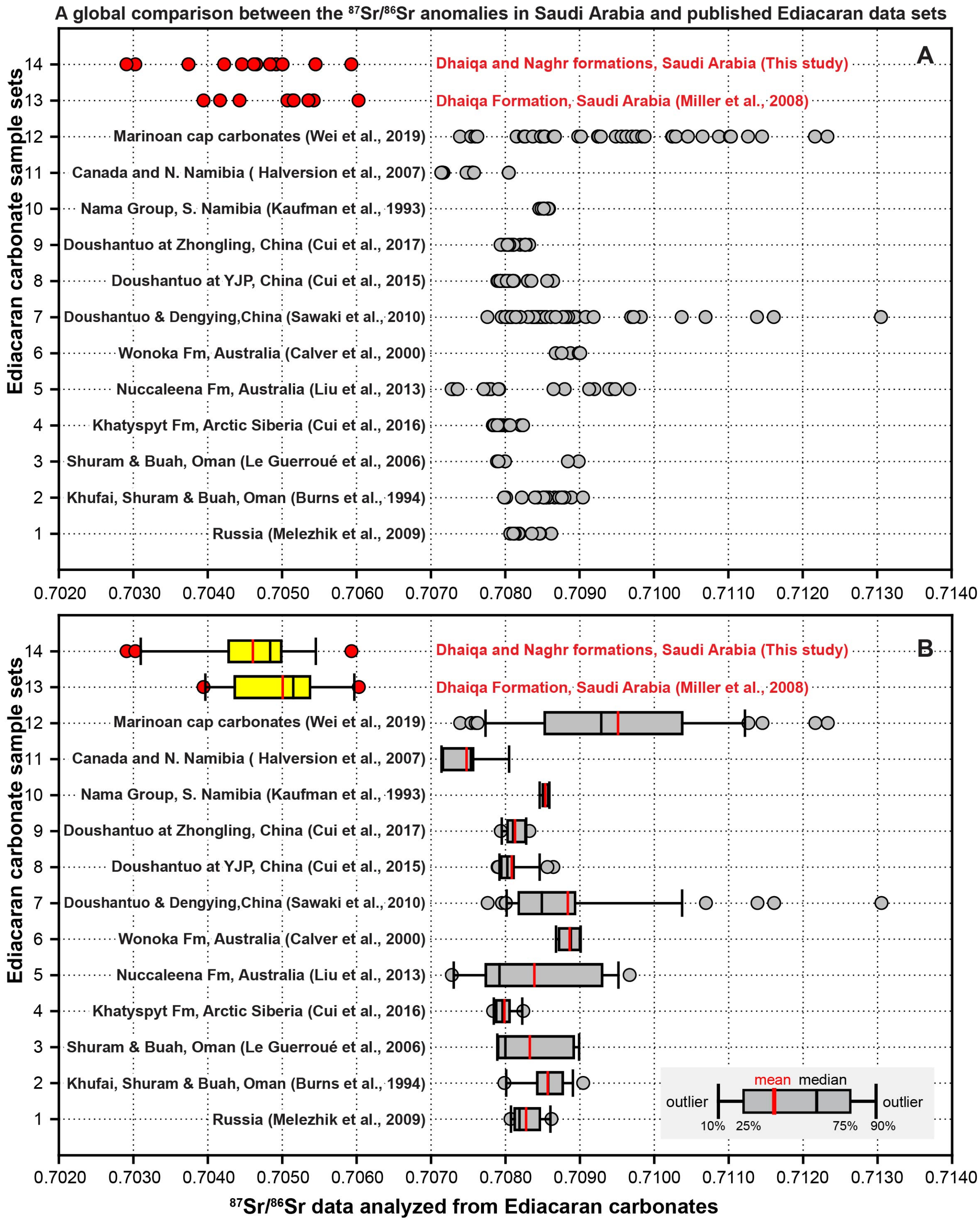

Figure 2. A global comparison between the $^{87}Sr/^{86}Sr$ data in Saudi Arabia (highlighted as red dots and yellow boxes) and the published data from other regions. Panel A showing all the compiled

data points; Panel B showing box plots. Data source: 1-Ediacaran strata in Siberia, Russia (Melezhik et al., 2009); 2-Khufai, Shuram, and Buah formations in Oman (Burns et al., 1994); 3-Shuram, and Buah formations in Oman (Le Guerroué et al., 2006); 4-Khatyspyt Formation in Arctic Siberia, Russia (Cui et al., 2016a); 5-Nuccaleena Formation, Australia (Liu et al., 2013); 6-Wonoka Formation, Australia (Calver, 2000); 7-Doushantuo and Dengying formations in the Three Gorges area, South China (Sawaki et al., 2010); 8-Doushantuo Formation at Yangjiaping (Cui et al., 2015); 9-Doushantuo Formation at Zhongling (Cui et al., 2017); 10-Nama Group, southern Namibia (Kaufman et al., 1993); 11-Maieberg Formation, northern Namibia and Hayhook Formation of the Mackenzie Mountains, Canada (Halverson et al., 2005; Halverson et al., 2007); 12-Marinoan cap carbonates in Keilberg Member of Nanibia, Doushantuo Formation of South China, and the Sugetbrak Formation of NW China (Wei et al., 2019a);13-Dhaiqa Formation, Saudi Arabia (Miller et al., 2008);14-Dhaiqa and Naghr formations, Saudi Arabia (this study).

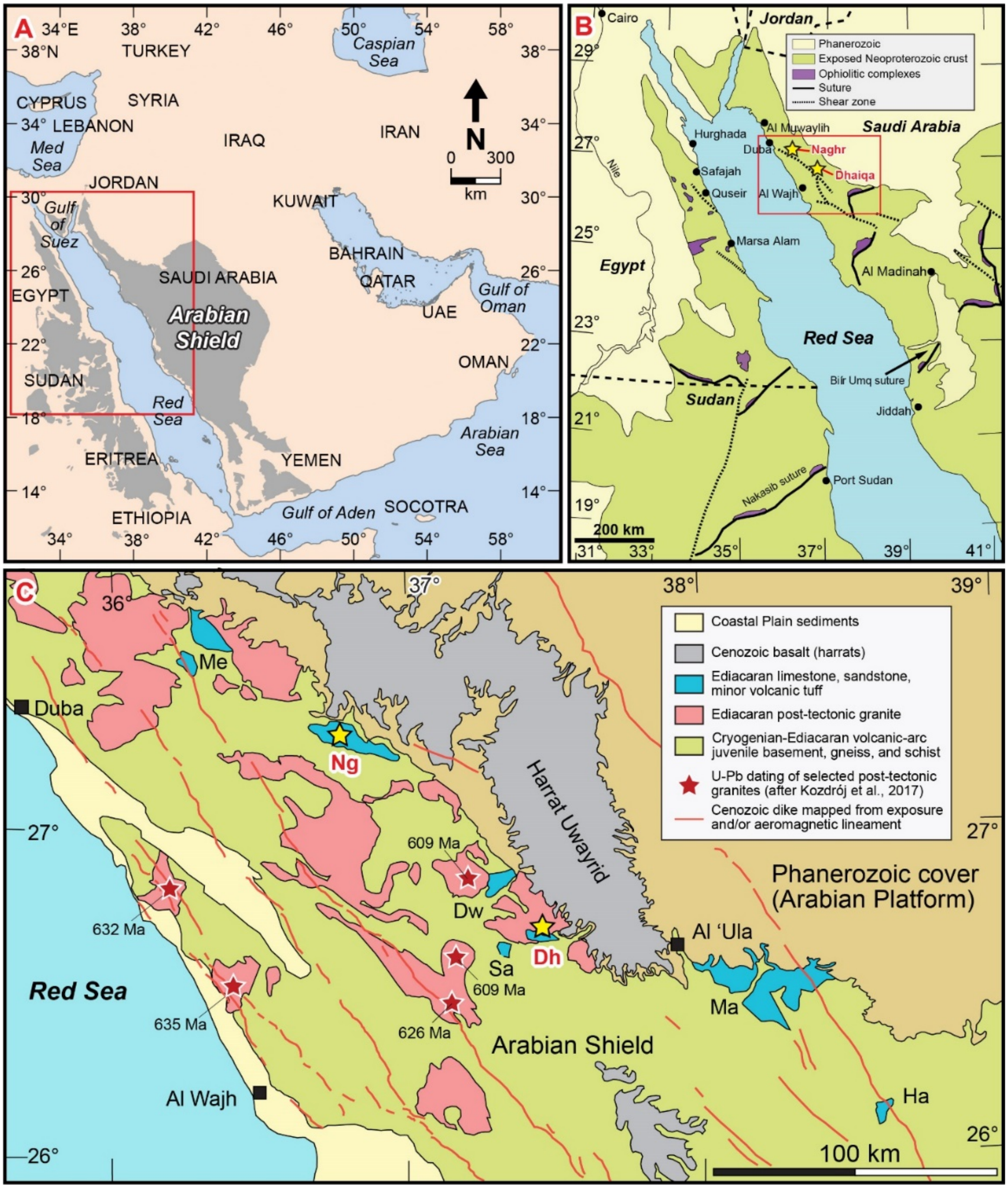

Figure 3. (A) Map of the Arabian Shield (highlighted in gray). Map modified after Al-Husseini (2011). (B) Locality of the two studied areas (labelled as yellow stars). Map modified after Stern

et al. (2011). (C) Ediacaran basins named after principal formations. The two studied basins for geochemical analyses in this study are labelled as yellow stars. Ng = Naghr basin; Dh = Dhaiqa basin; Dw = Dawqah basin; Ha = Hamra basin; Ma = Mashad basin; Me = Meddan basin; Sa = Salih basin. Source of the U-Pb age data (red stars): Kozdrój et al. (2018).

453

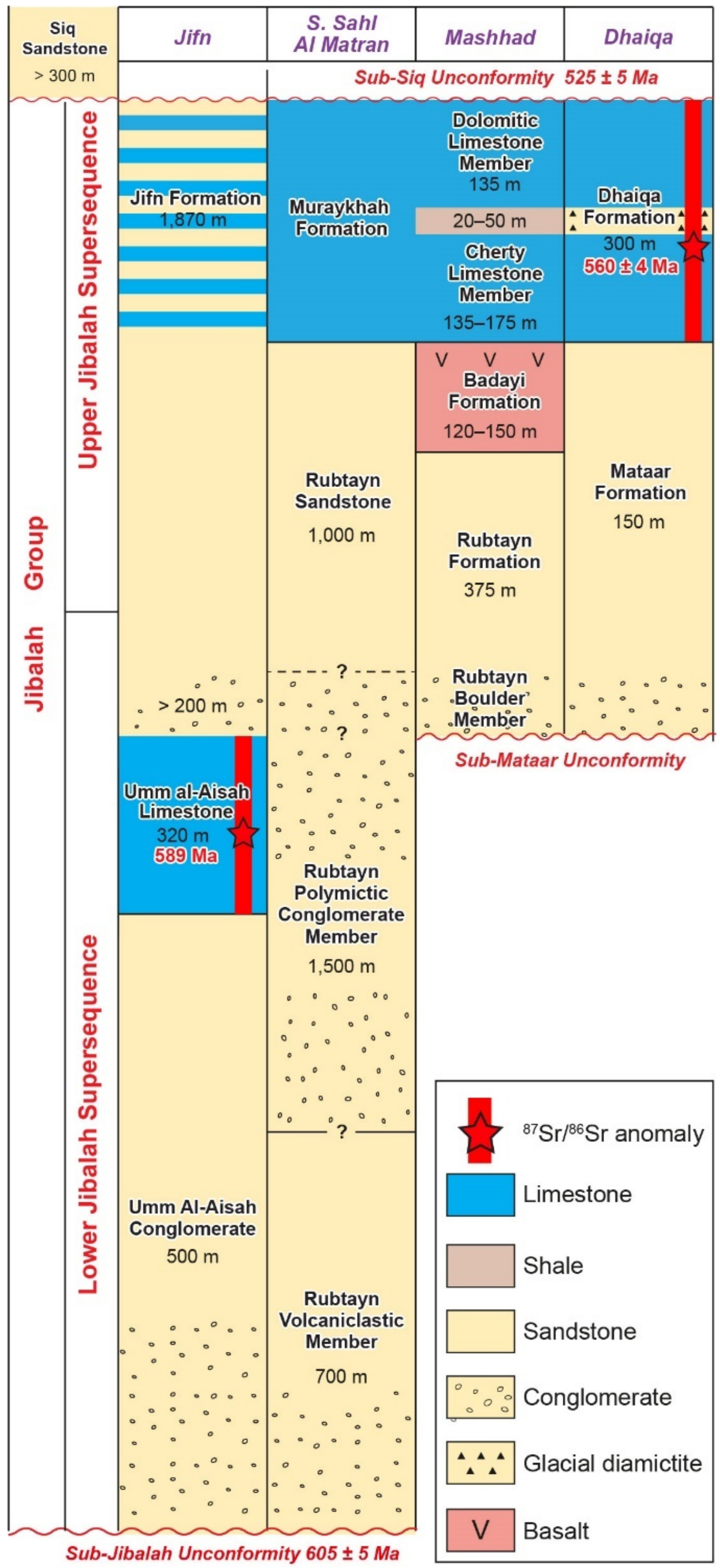

Siq Sandstone
> 300 m
Jifn
S. Sahl Al Matran
Mashhad
Dhaiqa
Sub-Siq Unconformity 525 ± 5 Ma
Jibalah Group
Upper Jibalah Supersequence
Lower Jibalah Supersequence
Jifn Formation
1,870 m
Muraykhah Formation
Dolomitic Limestone Member
135 m
20–50 m
Cherty Limestone Member
135–175 m
Dhaiqa Formation
300 m
560 ± 4 Ma
Badayi Formation
120–150 m
Rubtayn Sandstone
1,000 m
Rubtayn Formation
375 m
Mataar Formation
150 m
Rubtayn Boulder Member
> 200 m
Sub-Mataar Unconformity
Umm al-Aisah Limestone
320 m
589 Ma
Rubtayn Polymictic Conglomerate Member
1,500 m
Umm Al-Aisah Conglomerate
500 m
Rubtayn Volcaniclastic Member
700 m
Sub-Jibalah Unconformity 605 ± 5 Ma
$^{87}Sr/^{86}Sr$ anomaly
Limestone
Shale
Sandstone
Conglomerate
Glacial diamictite
Basalt

Figure 4. Stratigraphic scheme of the Ediacaran Jibalah Group in the Arabian Shield. Modified after Al-Husseini (2014). $^{87}Sr/^{86}Sr$ anomalies that are significantly decoupled from the typical Ediacaran seawater values have been found in the Umm al-Aisah Formation (Halverson et al., 2013a; Halverson et al., 2013b) and the Dhaiqa Formation (Miller et al., 2008 and this study).

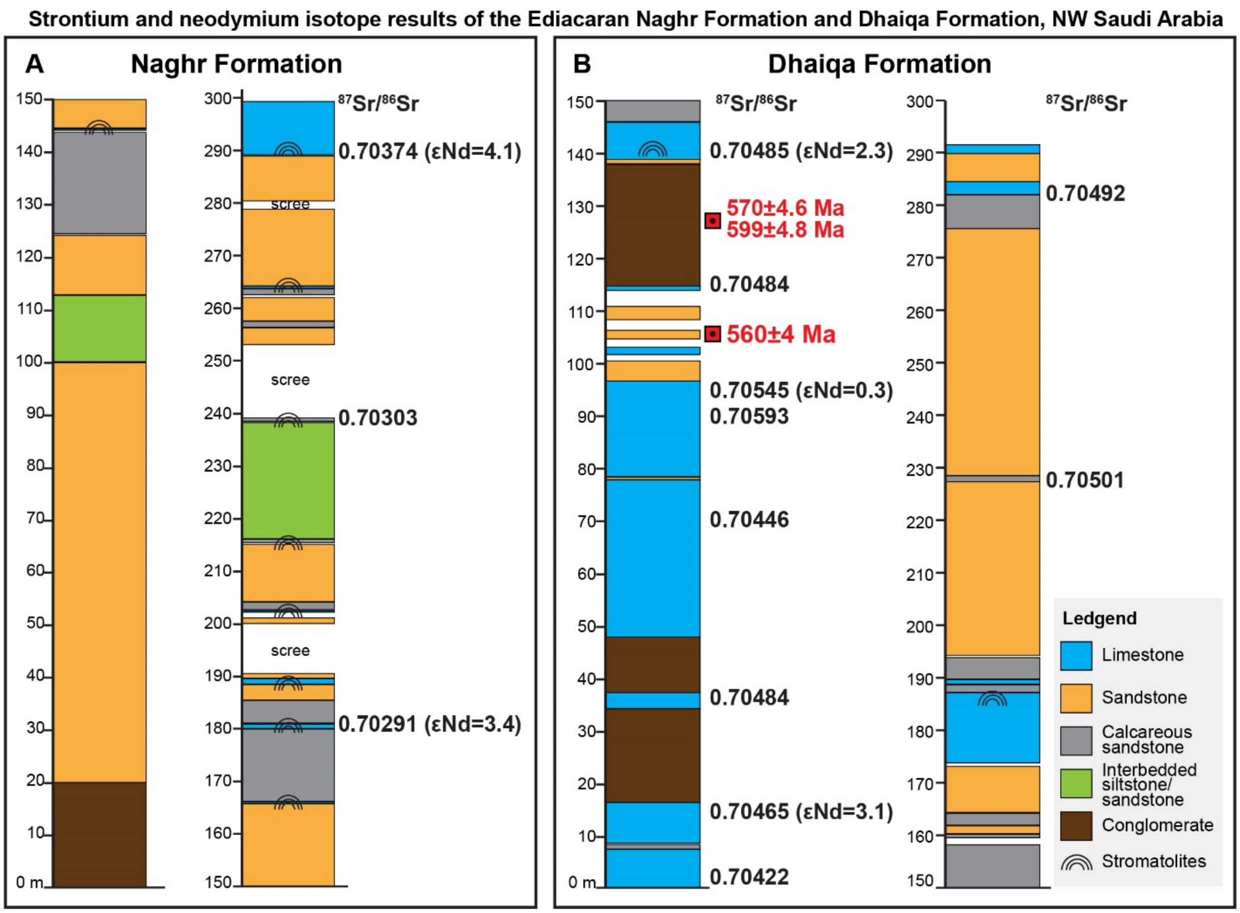

Figure 5. Lithology columns of (A) the Ediacaran Naghr Formation and (B) the Ediacaran Dhaiqa Formation. Strontium ($^{87}Sr/^{86}Sr$) and neodymium isotope $\varepsilon Nd_{carbonate}(t=560Ma)$ data newly reported in this study are shown alongside the lithology columns. All the Sr and Nd isotope data can be found in the online supplementary material. The age 560 ± 4 Ma is the youngest age of detrital zircons extracted from that interval, which represents the maximum depositional age

(Vickers-Rich et al., 2010; Vickers-Rich et al., 2013). The ages of 599 ± 4.8 Ma and 570 ± 4.6 Ma were measured from the core and the rim of a single detrital zircon, respectively (Miller et al., 2008).

Figure 6. Field photos of the Ediacaran Naghr Formation, NW Saudi Arabia. (A) Overview of the Naghr Formation in the field. (B) Tepee structures in the Naghr Formation. Pen as scale. (C) Possible drop stone within the diamictite interval of the Naghr Formation. Hammer as scale. (D) Basalt screes near the outcrops of the Naghr Formation. More field images of the studied section can be found in Vickers-Rich et al. (2010).

Figure 7. (A–C) Field photos of the Ediacaran Dhaiqa Formation, NW Saudi Arabia. (D) A closer view of the Dhaiqa Formation. More field images of the studied section can be found in Vickers-Rich et al. (2010) and Vickers-Rich et al. (2013).

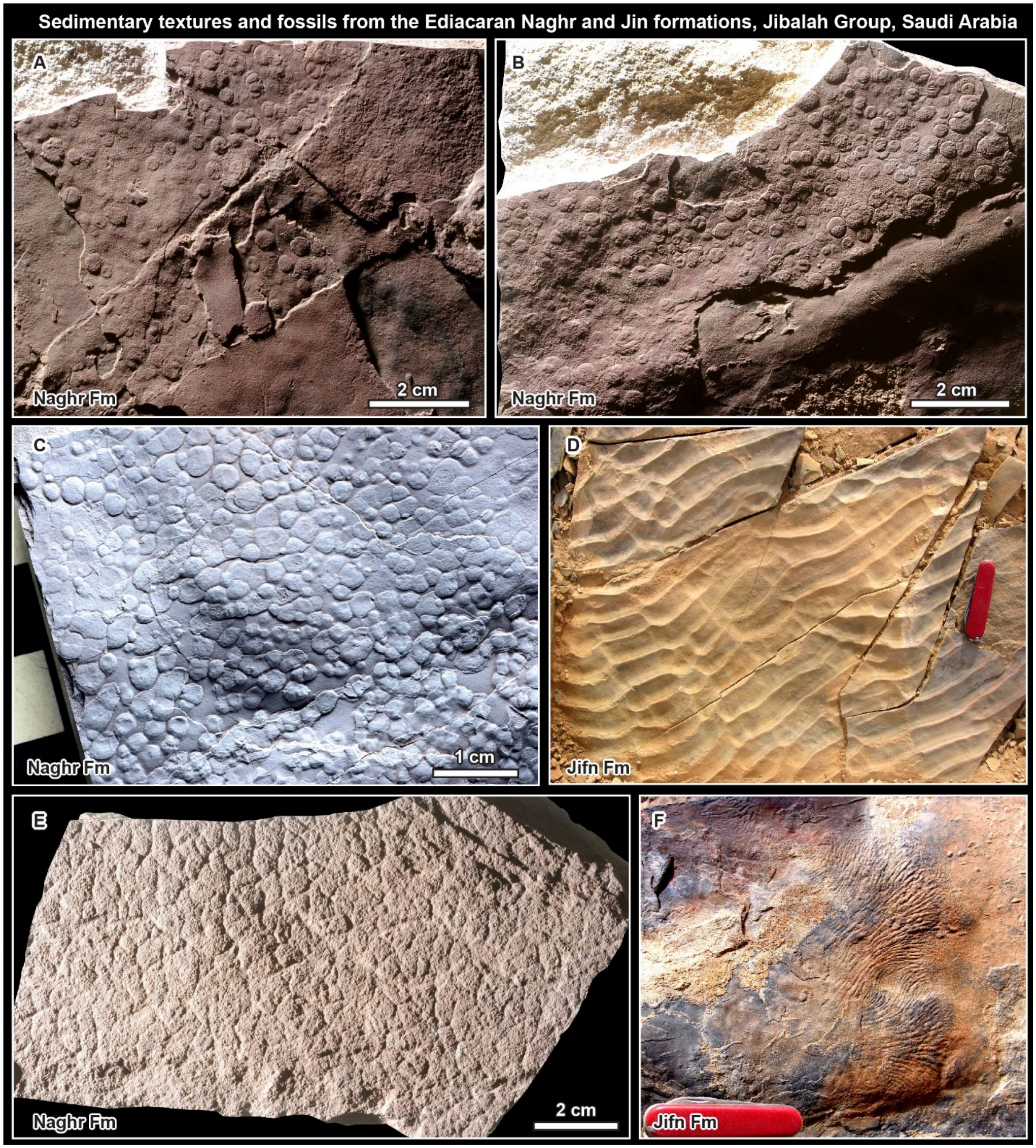

Figure 8. Sedimentary textures and fossils from the Ediacaran Naghr and Jifn formations, Saudi Arabia. **(A–C)** Large spherical colonies of cyanobacteria *Beltanelliformis minutae*. **(D)** Ripple marks; **(E)** Elephant-skin textures, indicating the existence of microbial mats on depositional

surfaces. **(F)** Microbial texture *Arumberia* sp. Swiss army knife (95mm in length) as scale in D and F.

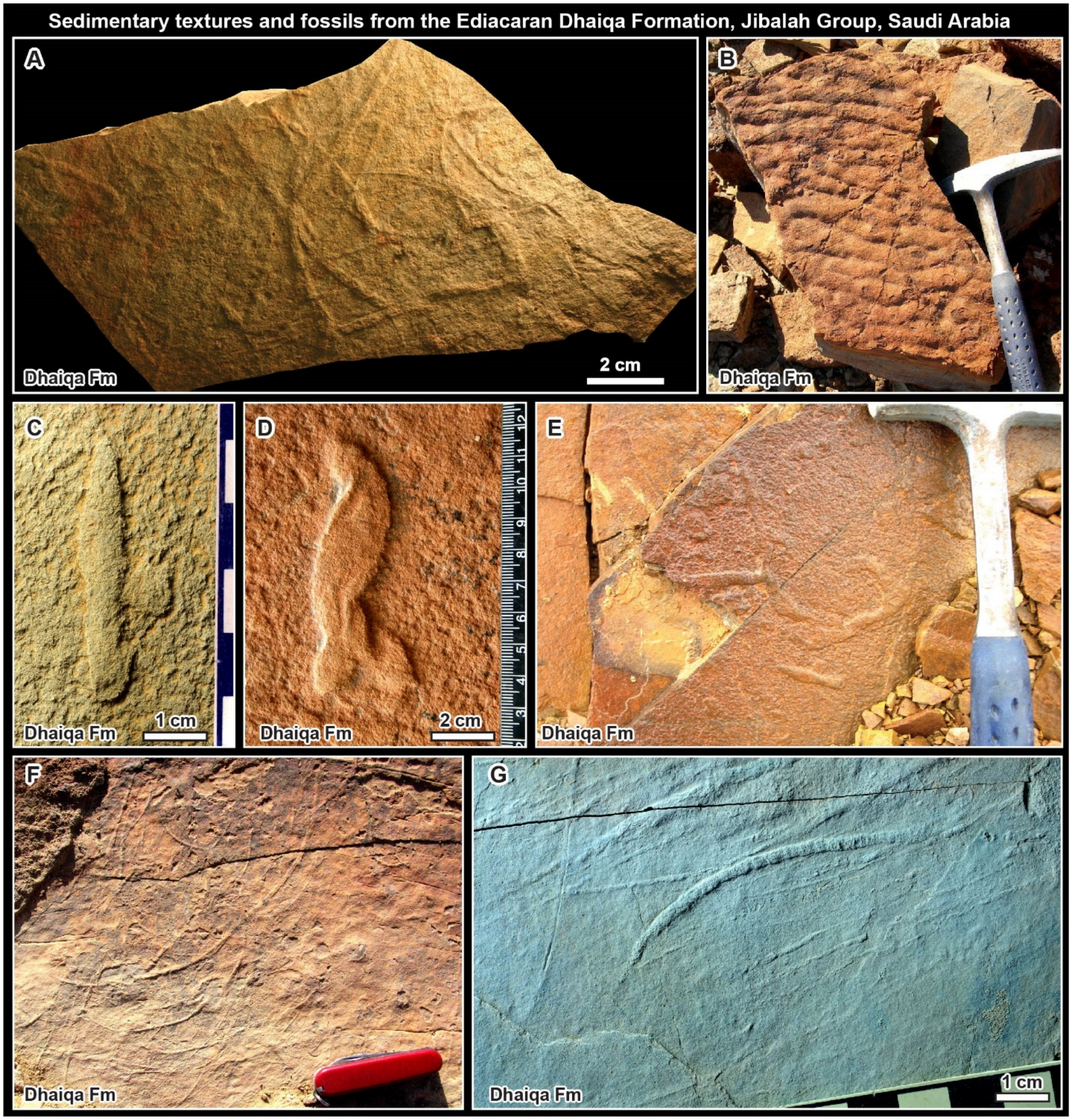

Figure 9. Sedimentary textures and fossils from the Ediacaran Dhaiqa Formation, Saudi Arabia. **(A)** Algal remains of *Harlaniella ingriana*. **(B)** Ripple marks possibly bounded by microbial mats. **(C–D)** Samples found directly below a volcanic ash layer, which look similar to the iconic Ediacara-type fossil *Charniodiscus,* though detailed features are lacking. (**E**) Body remains of uncertain attribution. **(F)** Algal remains of *Harlaniella ingriana*. (**G**) A segmented tubular form of *Harlaniella.* Swiss army knife (95mm in length) as scale in F. Images modified from Vickers-Rich et al. (2010); Vickers-Rich et al. (2013).

Figure 10. Sedimentary textures and fossils from the Ediacaran Muraykhah Formation and the Cambrian Sig sandstone Formation, Saudi Arabia. **(A, B)** Possible metazoan trace fossils. (**C**) Concentric textures that look similar to the *Eoandromeda octobrachiata* fossils reported from China and Australia (Zhu et al., 2008), but can also be simply abiotic sedimentological textures (e.g., nodules). **(D)** Algal remains of *Harlaniella ingriana*. (**E**) Large spherical colonies of cyanobacteria

Beltanelliformis. (**F**) Possible metazoan trace fossils. (**G**) *Cruziana* trails in the Sajir Member of the Cambrian Siq Sandstone interval. Coin (red arrow) as scale. Images modified from Vickers-Rich et al. (2010); Vickers-Rich et al. (2013).

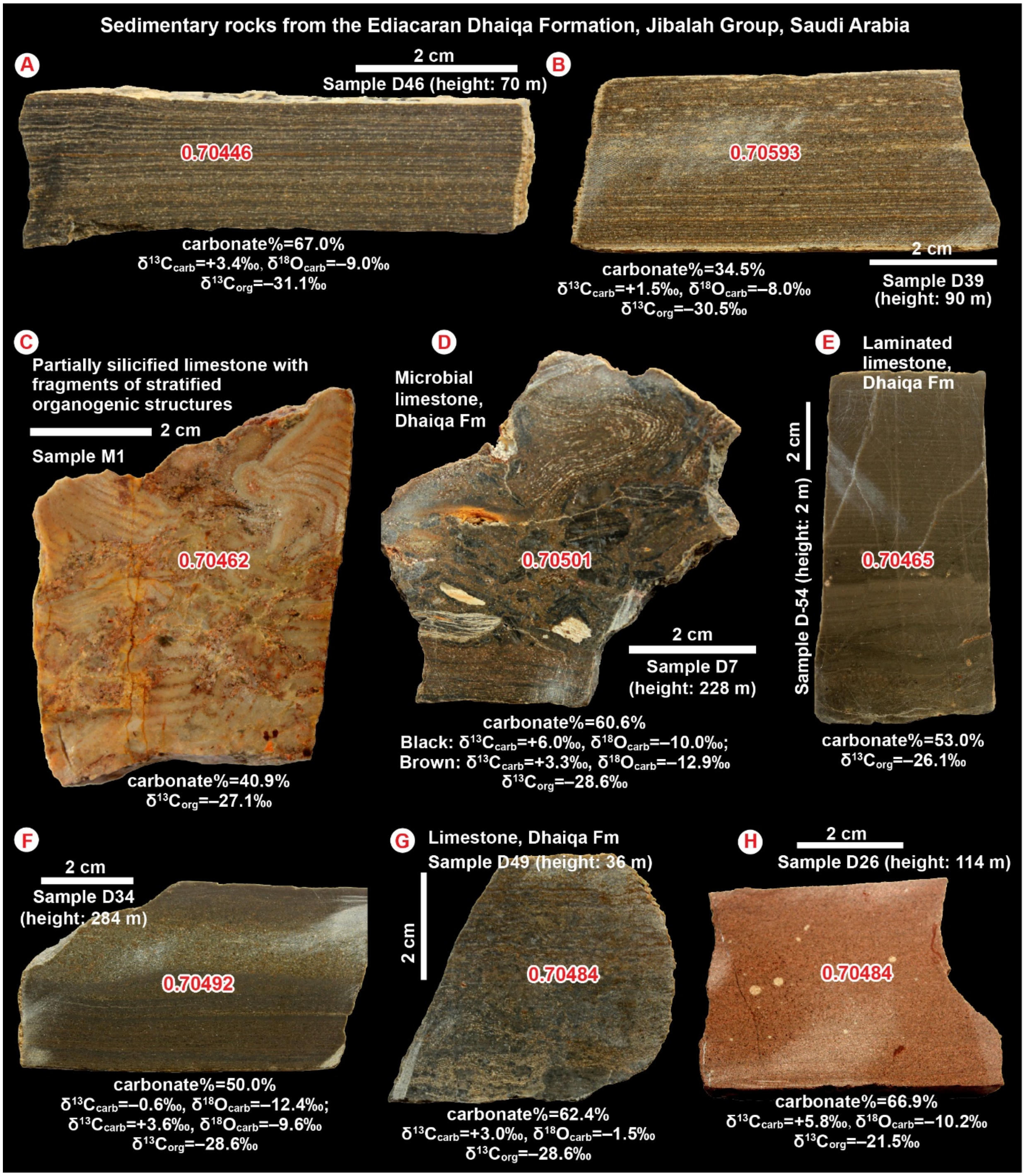

Figure 11. $^{87}Sr/^{86}Sr$ compositions (in red) of the limestone or calcareous sandstone samples from the Ediacaran Dhaiqa Formation, NW Saudi Arabia. The values of carbonate content (wt%), $\delta^{13}C_{carb}$ (VPDB, ‰), $\delta^{18}O_{carb}$ (VPDB, ‰), and $\delta^{13}C_{org}$ (VPDB, ‰) are provided when available.

(A) Sample D46; (B) Sample D39; (C) Sample D-M1; (D) Sample D7; (E) Sample D54; (F) Sample D34; (G) Sample D49; (H) Sample D26. Samples were acidified by 0.5 M weak acid so that only the carbonate portion was extracted for $^{87}Sr/^{86}Sr$ and elemental concentration analyses. Stratigraphic height of each sample is also provided when available. All the data can be found in the online supplementary materials.

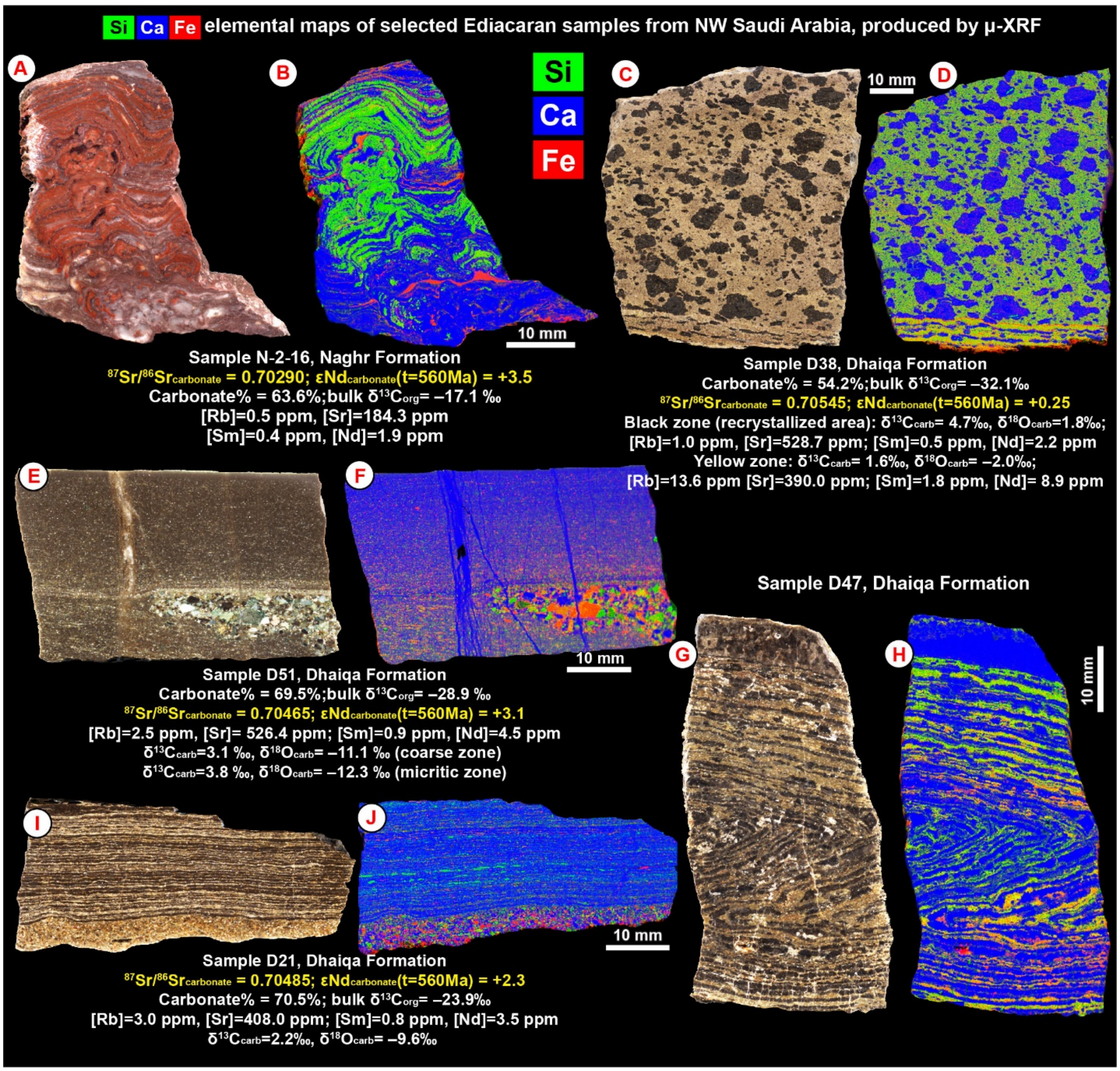

Figure 12. continued.

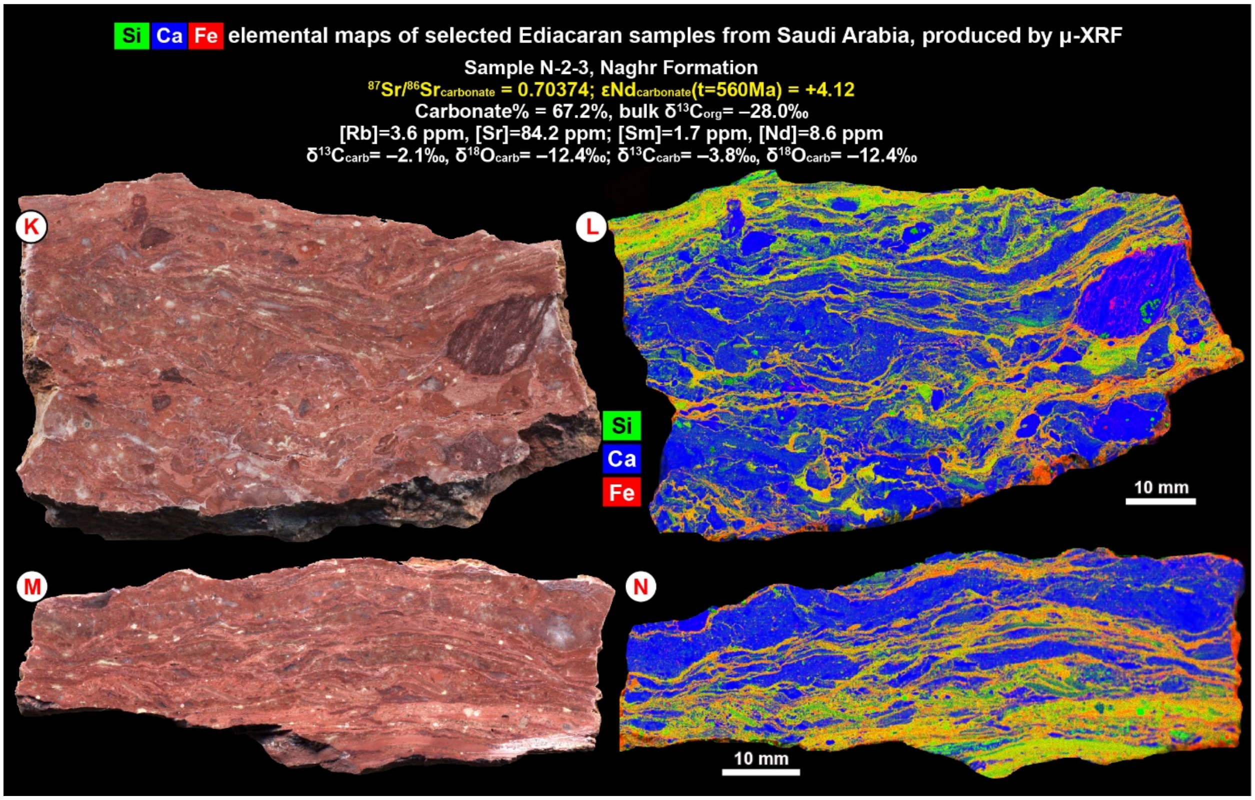

Figure 12. Polished rock slab images and coupled Si (green)–Ca (blue)–Fe (red) elemental maps produced by μXRF. Geochemical compositions, including $^{87}Sr/^{86}Sr$ and εNd(t=560Ma) values, are also provided when available. All the samples were collected from the Ediacaran Naghr and Dhaiqa formations on the Arabian Shield. (A, B) Sample N-2-16, Naghr Formation; (C, D) Sample D38, Dhaiqa Formation; (E, F) Sample D51, Dhaiqa Formation; (G, H) Sample D47, Dhaiqa Formation; (I, J) Sample D21, Dhaiqa Formation; (K–N) Sample N-2-3, Naghr Formation. Samples were acidified by 0.5 M weak acid so that only the carbonate portion was extracted for Sr and Nd isotopic and elemental concentration analyses. Note that all the analyzed samples yield anomalously low $^{87}Sr/^{86}Sr$ values and anomalously high εNd(t=560Ma) values compared with the typical Ediacaran seawater values. All the data can be found in the online supplementary materials.

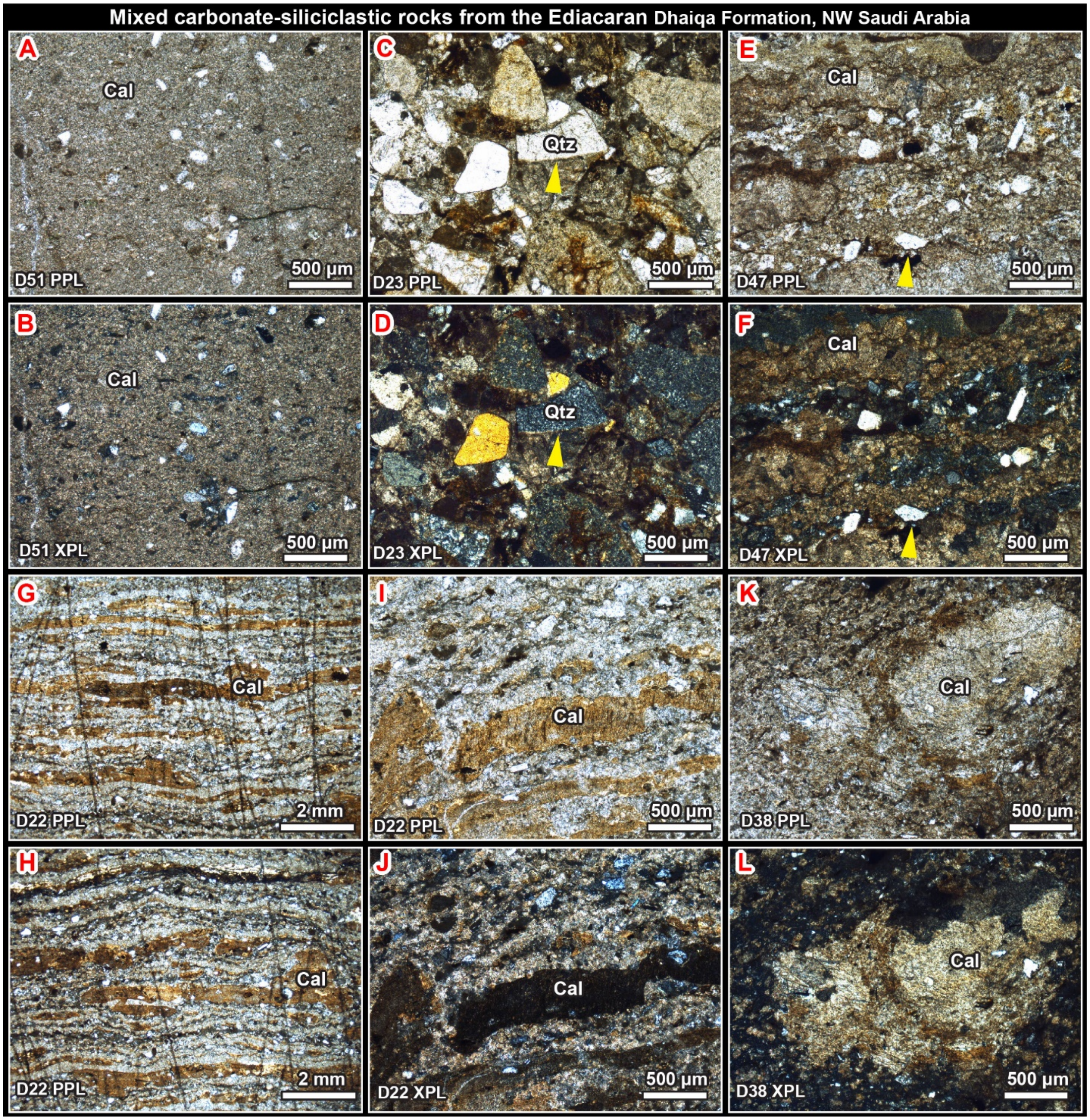

Figure 13. Petrographic images under plane polarized light (PPL), cross polarized light (XPL). Sample names are provided in the lower left. (A, B) Limestone sample D51 with abundant detrital quartz grains; (C, D) Sandstone sample D23 with abundant angular quartz grains (arrows); (E–J)

Laminated siliciclastic and calcite samples D47 and D22 with abundant angular quartz grains (arrows); (K, L) Carbonate sample D38 with large (up to ca. 10 mm) carbonate crystals within siliciclastic matrix. See Figure 11 for rock slab images of sample D38, D47, D51. Corresponding rock slab images of all the samples can be found in the online supplementary materials.

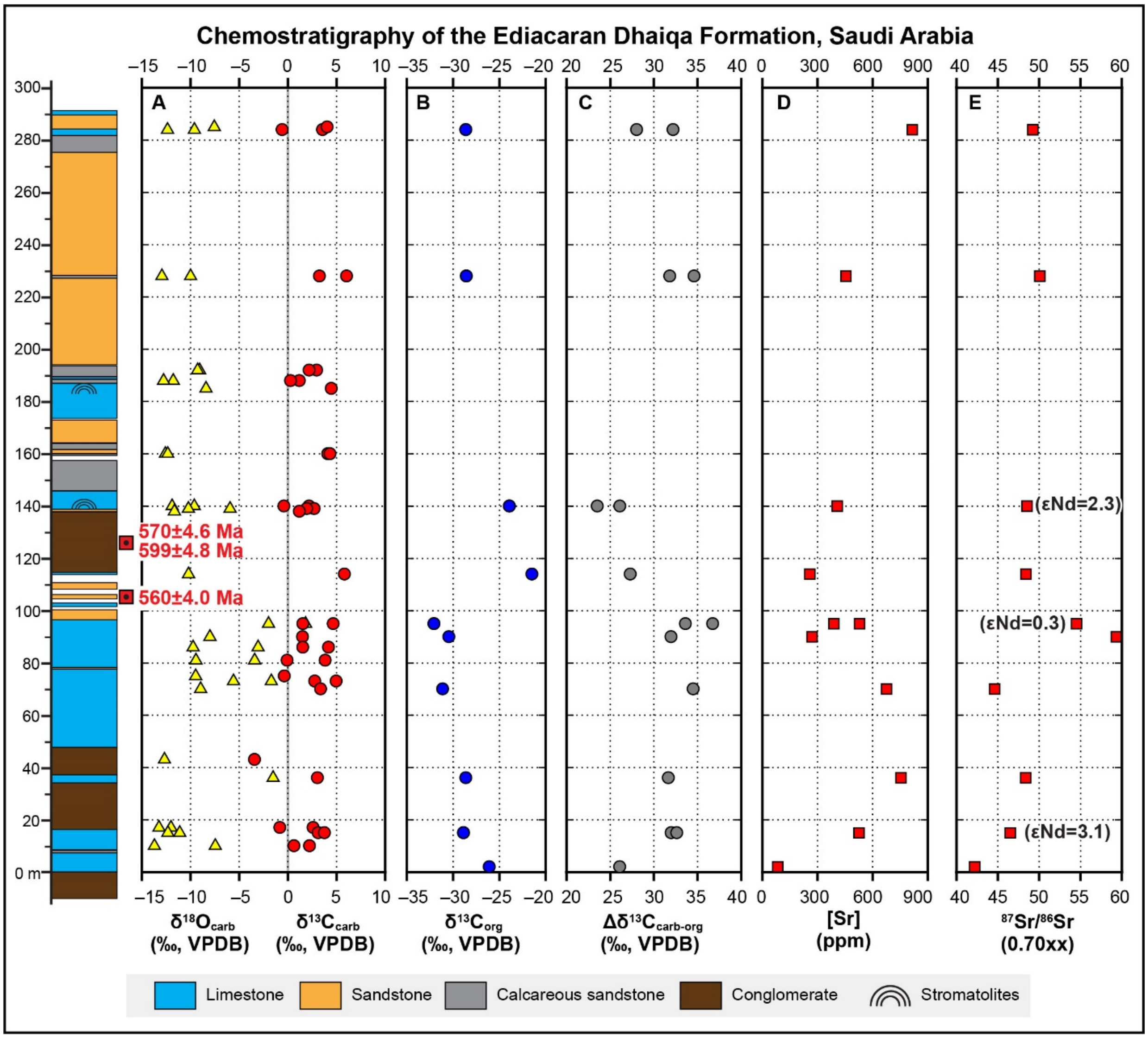

Figure 14. Litho- and chemostratigraphy of the Ediacaran Dhaiqa Formation. The geochemical data include (A) carbonate carbon ($\delta^{13}C_{carb}$) and oxygen ($\delta^{18}O_{carb}$) isotopes, (B) organic carbon

isotopes ($\delta^{13}C_{org}$), (C) carbon isotope fractionations ($\Delta\delta^{13}C_{carb-org}$), (D) strontium concentrations ([Sr] in ppm), (E) strontium isotope ratios ($^{87}Sr/^{86}Sr$). Measured neodymium isotope data $\varepsilon Nd_{carbonate}(t=560\ Ma)$ are also provided in panel E. The age 560 ± 4.0 Ma is the youngest age of detrital zircons extracted from that interval, which represents the maximum depositional age (Vickers-Rich et al., 2010; Vickers-Rich et al., 2013). The ages of 599 ± 4.8 Ma and 570 ± 4.6 Ma were measured from the core and the rim of a single detrital zircon, respectively (Miller et al., 2008).

545

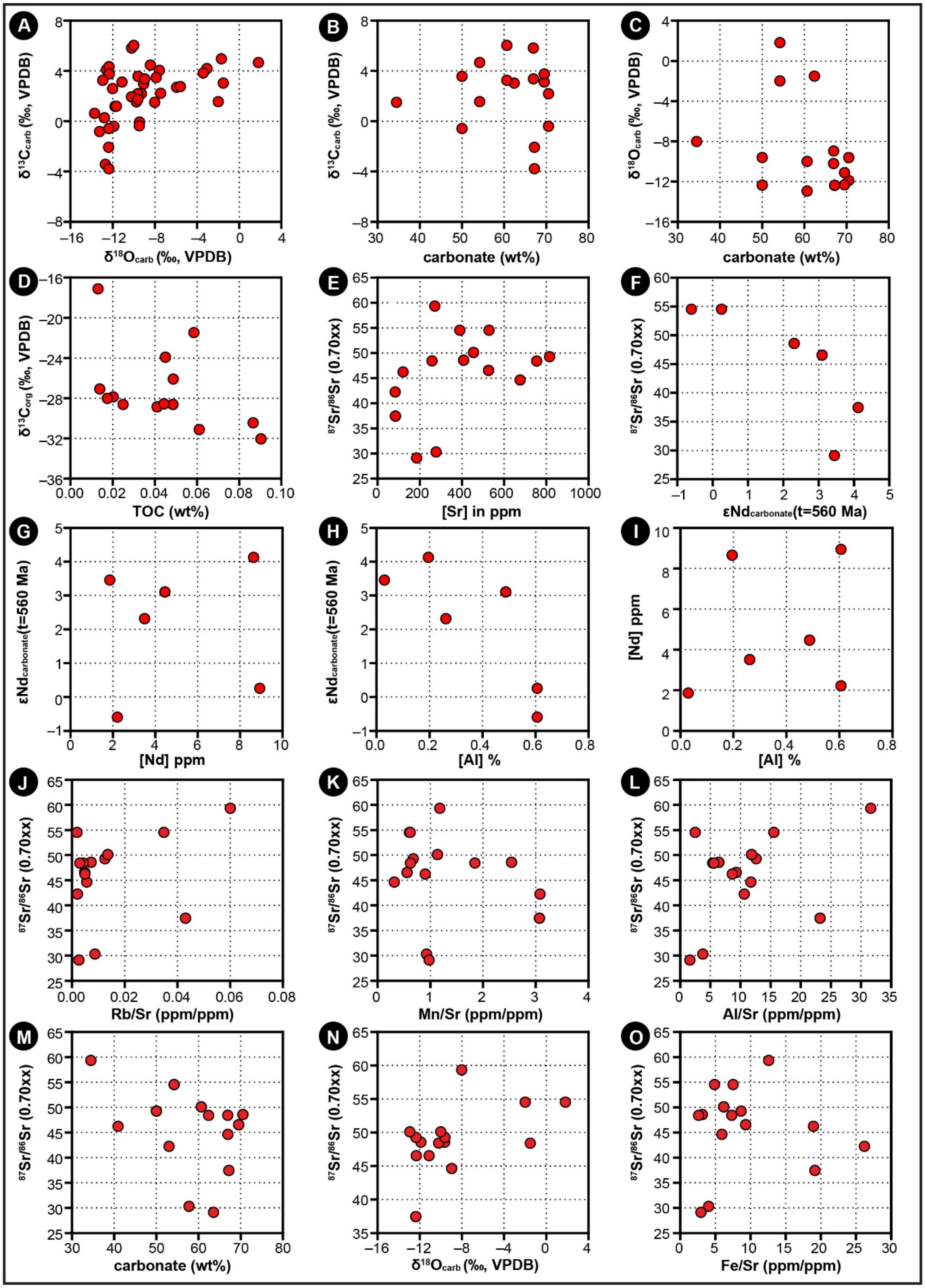

A
B
C
D
E
F
G
H
I
J
K
L
M
N
O
δ¹³Ccarb (‰, VPDB)
δ¹⁸Ocarb (‰, VPDB)
carbonate (wt%)
δ¹⁸Ocarb (‰, VPDB)
δ¹³Corg (‰, VPDB)
TOC (wt%)
⁸⁷Sr/⁸⁶Sr (0.70xx)
[Sr] in ppm
εNdcarbonate(t=560 Ma)
[Nd] ppm
[Al] %
Rb/Sr (ppm/ppm)
Mn/Sr (ppm/ppm)
Al/Sr (ppm/ppm)
Fe/Sr (ppm/ppm)

Figure 15. Cross-plots of data measured in this study. All the data can be found in the online supplementary materials.

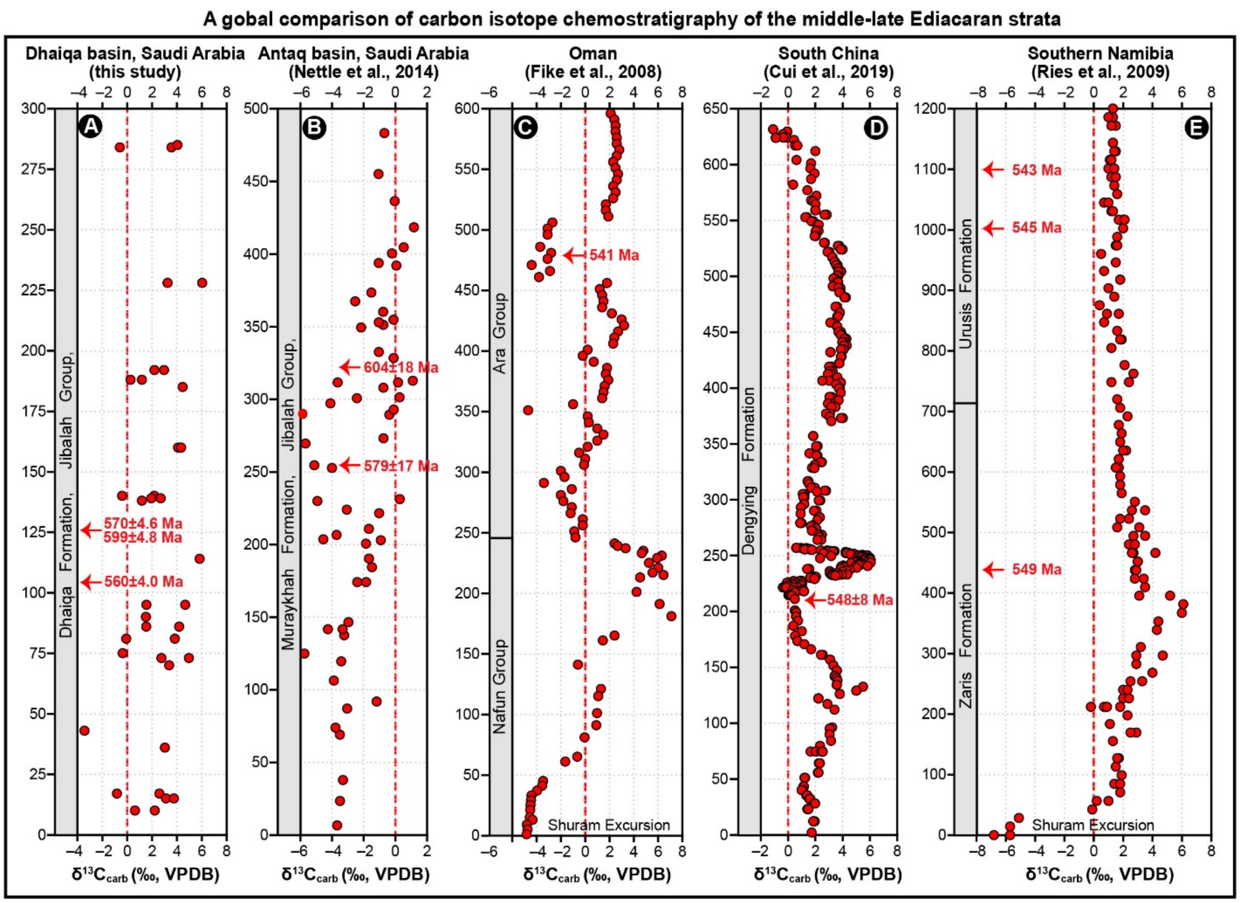

Figure 16. A global comparison of the carbon isotope chemostratigraphy of the middle- to late-Ediacaran strata. (A) Dhaiqa Formation of the Jibalah Group, Dhaiqa basin, Saudi Arabia (this study); (B) Muraykhah Formation of the Jibalah Group, Antaq basin, Saudi Arabia (Nettle et al., 2014); (C) Oman (Fike and Grotzinger, 2008); (D) Dengying Formation at the Gaojiashan section, South China (Cui et al., 2016b; Cui et al., 2019); (E) Nama Group in southern Namibia (Ries et al., 2009).

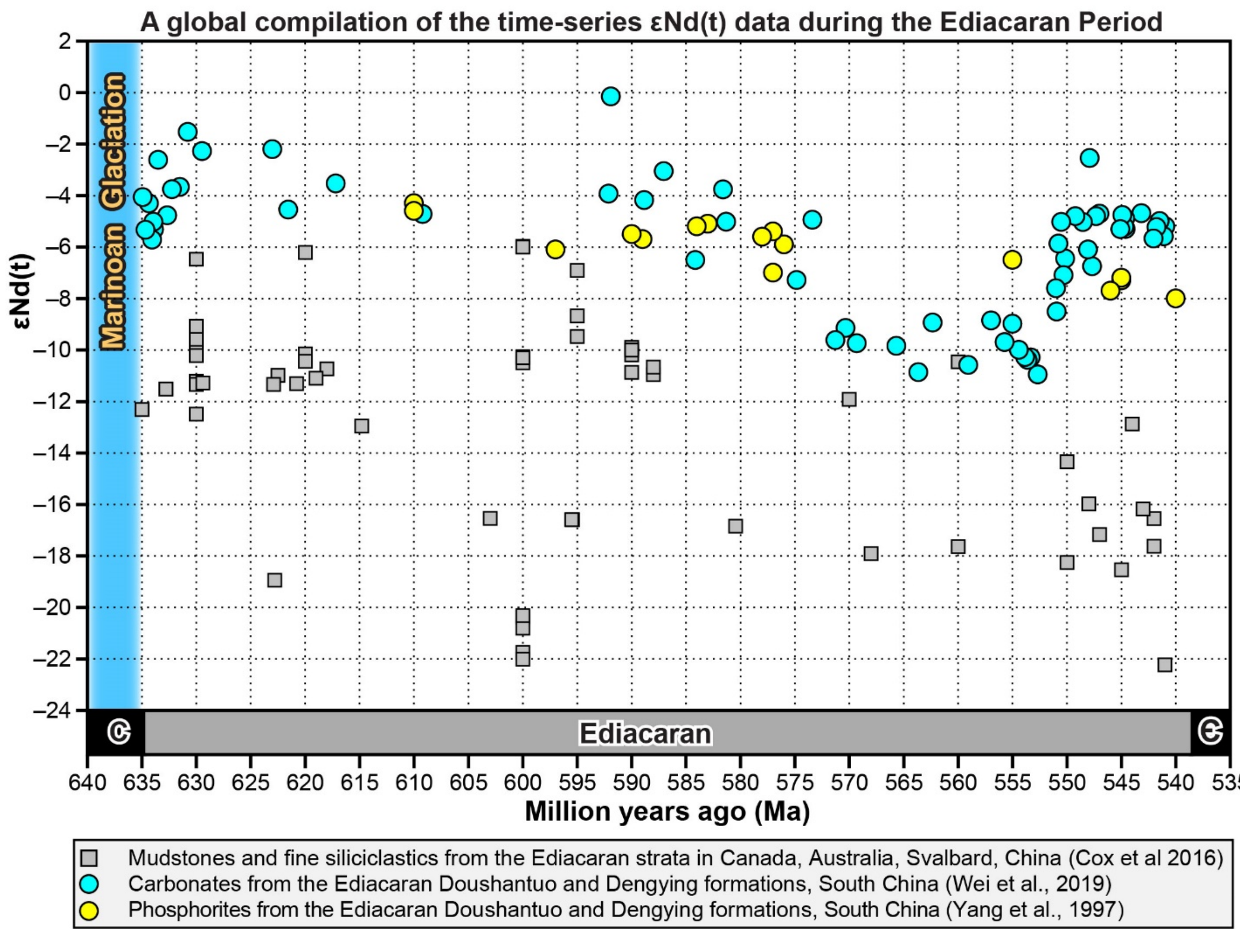

Figure 17. Reconstructed εNd(t) profile for the Ediacaran Period (ca. 635–538 Ma). Data source: phosphorites from the Doushantuo and Dengying formations in South China (Yang et al., 1997); mudstones and fine-grained siliciclastics in Canada, Australia, Svalbard, and China (Cox et al., 2016); carbonates from the Doushantuo and Dengying formations in South China (Wei et al., 2019b).

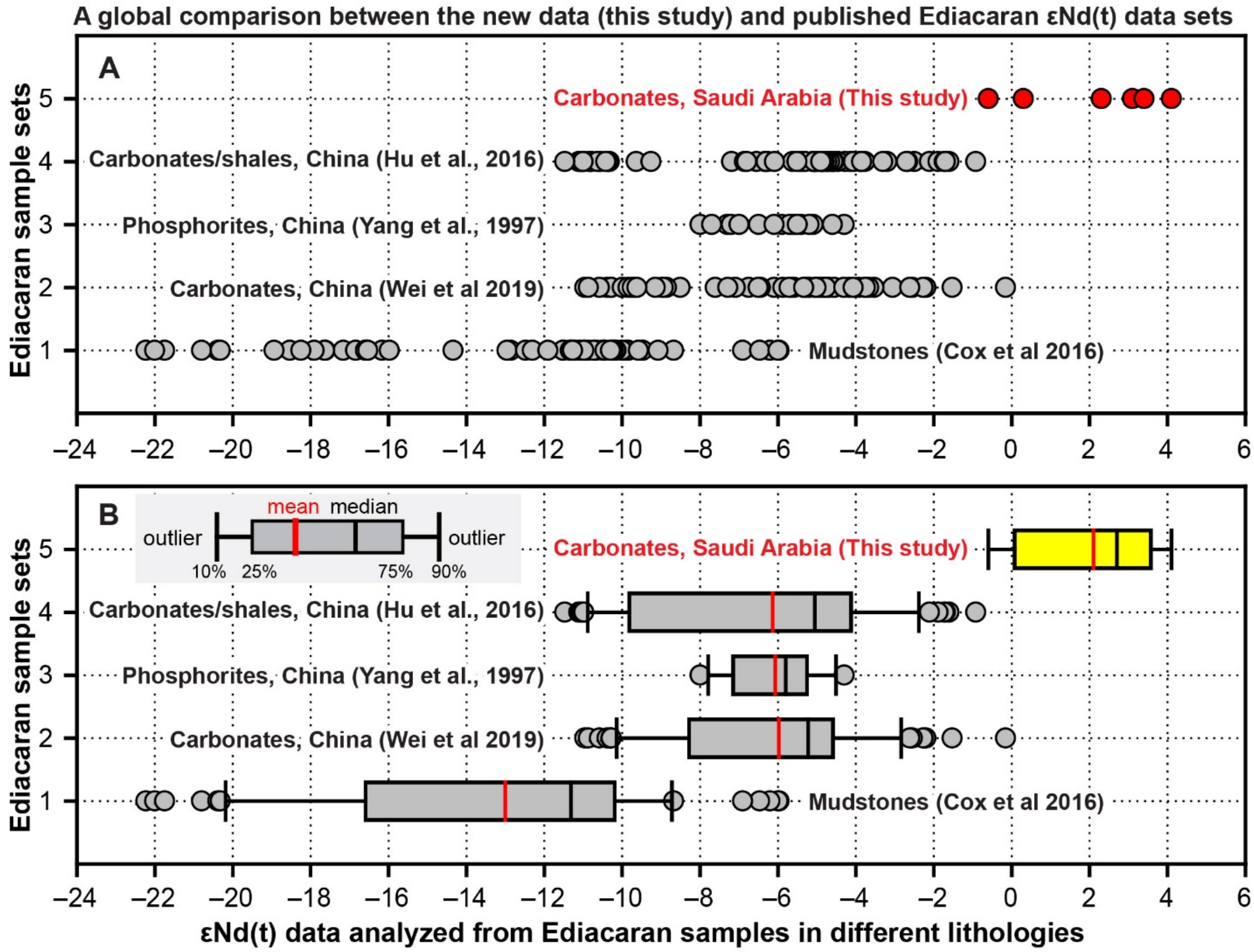

Figure 18. A global comparison between the new εNd(t) data in this study (highlighted as red dots and a yellow box) and the published data. Panel A showing all the compiled data points; Panel B showing box plots. Data source: 1-Mudstones or fine-grained siliciclastics from Ediacaran strata in Canada, Australia, Svalbard, and China (Cox et al., 2016); 2-Carbonates from the Ediacaran Doushantuo and Dengying formations, South China (Wei et al., 2019b); 3-Phosphorites from the Ediacaran Doushantuo and Dengying formations, South China (Yang et al., 1997); 4-Carbonates and shales from the Ediacaran Doushantuo Formation, South China (Hu et al., 2016); 5-Ediacaran Dhaiqa and Naghr formations, Saudi Arabia (this study).

References

Al-Husseini, M., 2014. Ediacaran–Cambrian Middle East Geologic Time Scale 2014: Proposed correlation of Oman's Abu Mahara Supergroup and Saudi Arabia's Jibalah Group. Geoarabia, 19: 107–132

Al-Husseini, M.I., 2011. Late Ediacaran to early Cambrian (Infracambrian) Jibalah Group of Saudi Arabia. GeoArabia, 16(3): 69–90

Alibo, D.S., Nozaki, Y., 1999. Rare earth elements in seawater: particle association, shale-normalization, and Ce oxidation. Geochimica et Cosmochimica Acta, 63(3–4): 363–372 https://doi.org/10.1016/s0016-7037(98)00279-8.

Allègre, C.J., Louvat, P., Gaillardet, J., Meynadier, L., Rad, S., Capmas, F., 2010. The fundamental role of island arc weathering in the oceanic Sr isotope budget. Earth and Planetary Science Letters, 292(1): 51–56 https://doi.org/10.1016/j.epsl.2010.01.019.

Allen, P.A., 2007. The Huqf Supergroup of Oman: Basin development and context for Neoproterozoic glaciation. Earth-Science Reviews, 84(3–4): 139-185 https://doi.org/10.1016/j.earscirev.2007.06.005.

Asmeron, Y., Jacobsen, S.B., Knoll, A.H., Butterfield, N.J., Swett, K., 1991. Strontium isotopic variations of Neoproterozoic seawater: implications for crustal evolution. Geochim. Cosmochim. Acta, 55: 2883–2894 https://doi.org/10.1016/0016-7037(91)90453-c.

Baldridge, W.S., Eyal, Y., Bartov, Y., Steinitz, G., Eyal, M., 1991. Miocene magmatism of sinai related to the opening of the red sea. Tectonophysics, 197(2): 181–201 https://doi.org/10.1016/0040-1951(91)90040-Y.

Banner, J.L., 1995. Application of the trace element and isotope geochemistry of strontium to studies of carbonate diagenesis. Sedimentology, 42(5): 805–824 https://doi.org/10.1111/j.1365-3091.1995.tb00410.x.

Be'eri-Shlevin, Y., Katzir, Y., Blichert-Toft, J., Kleinhanns, I.C., Whitehouse, M.J., 2010. Nd–Sr–Hf–O isotope provinciality in the northernmost Arabian–Nubian Shield: implications for crustal evolution. Contributions to Mineralogy and Petrology, 160(2): 181–201 https://doi.org/10.1007/s00410-009-0472-8.

Berglund, M., Wieser, M.E., 2011. Isotopic compositions of the elements 2009 (IUPAC Technical Report). Pure and Applied Chemistry, 83(2): 397–410 https://doi.org/10.1351/PAC-REP-10-06-02.

Bobrovskiy, I., Hope, J.M., Krasnova, A., Ivantsov, A., Brocks, J.J., 2018. Molecular fossils from organically preserved Ediacara biota reveal cyanobacterial origin for Beltanelliformis. Nature Ecology & Evolution, 2(3): 437–440 https://doi.org/10.1038/s41559-017-0438-6.

Bold, U., Smith, E.F., Rooney, A.D., Bowring, S.A., Buchwaldt, R., Dudás, F.Ő., Ramezani, J., Crowley, J.L., Schrag, D.P., Macdonald, F.A., 2016. Neoproterozoic stratigraphy of the Zavkhan terrane of Mongolia: The backbone for Cryogenian and early Ediacaran chemostratigraphic records. American Journal of Science, 316(1): 1–63 https://doi.org/10.2475/01.2016.01.

Bristow, T.F., Bonifacie, M., Derkowski, A., Eiler, J.M., Grotzinger, J.P., 2011. A hydrothermal origin for isotopically anomalous cap dolostone cements from south China. Nature, 474(7349): 68–71 https://doi.org/10.1038/nature10096.

Bristow, T.F., Kennedy, M.J., Derkowski, A., Droser, M.L., Jiang, G., Creaser, R.A., 2009. Mineralogical constraints on the paleoenvironments of the Ediacaran Doushantuo

Formation. Proceedings of the National Academy of Sciences, 106(32): 13190–13195 https://doi.org/10.1073/pnas.0901080106.
Broecker, W., 2003. The oceanic $CaCO_3$ cycle. In: Holland, H.D., Turekian, K.K. (Eds.), Treatise on Geochemistry. Elsevier, Oxford, pp. 529–549 https://doi.org/10.1016/B0-08-043751-6/06119-3.
Broecker, W.S., Peng, T.H., 1982. Tracers in the Sea. Eldigio Press, Lamont Doherty Geological Observatory, Palisades, NY.
Burns, S.J., Haudenschild, U., Matter, A., 1994. The strontium isotopic composition of carbonates from the late Precambrian (~560–540 Ma) Huqf Group of Oman. Chemical Geology, 111(1–4): 269–282 https://doi.org/10.1016/0009-2541(94)90094-9.
Calver, C.R., 2000. Isotope stratigraphy of the Ediacaran (Neoproterozoic III) of the Adelaide Rift Complex, Australia, and the overprint of water column stratification. Precambrian Research, 100(1–3): 121–150 https://doi.org/10.1016/s0301-9268(99)00072-8.
Camp, V.E., Roobol, M.J., 1989. The Arabian continental alkali basalt province: Part I. Evolution of Harrat Rahat, Kingdom of Saudi Arabia. Geological Society of America Bulletin, 101(1): 71–95 https://doi.org/10.1130/0016-7606(1989)101<0071:tacabp>2.3.co;2.
Chesson, L.A., Tipple, B.J., Mackey, G.N., Hynek, S.A., Fernandez, D.P., Ehleringer, J.R., 2012. Strontium isotopes in tap water from the coterminous USA. Ecosphere, 3(7): 1–17 https://doi.org/10.1890/ES12-00122.1.
Coleman, R.G., DeBari, S., Peterman, Z., 1992. A-type granite and the Red Sea opening. Tectonophysics, 204(1): 27–40 https://doi.org/10.1016/0040-1951(92)90267-A.
Collerson, K.D., Ullman, W.J., Torgersen, T., 1988. Ground waters with unradiogenic 87Sr/86Sr ratios in the Great Artesian Basin, Australia. Geology, 16(1): 59–63 https://doi.org/10.1130/0091-7613(1988)016<0059:GWWUSS>2.3.CO;2.
Cox, G.M., Halverson, G.P., Stevenson, R.K., Vokaty, M., Poirier, A., Kunzmann, M., Li, Z.-X., Denyszyn, S.W., Strauss, J.V., Macdonald, F.A., 2016. Continental flood basalt weathering as a trigger for Neoproterozoic Snowball Earth. Earth and Planetary Science Letters, 446: 89–99 https://doi.org/10.1016/j.epsl.2016.04.016.
Cui, H., Grazhdankin, D.V., Xiao, S., Peek, S., Rogov, V.I., Bykova, N.V., Sievers, N.E., Liu, X.-M., Kaufman, A.J., 2016a. Redox-dependent distribution of early macro-organisms: Evidence from the terminal Ediacaran Khatyspyt Formation in Arctic Siberia. Palaeogeography, Palaeoclimatology, Palaeoecology, 461: 122–139 https://doi.org/10.1016/j.palaeo.2016.08.015.
Cui, H., Kaufman, A.J., Xiao, S., Peek, S., Cao, H., Min, X., Cai, Y., Siegel, Z., Liu, X.M., Peng, Y., Schiffbauer, J.D., Martin, A.J., 2016b. Environmental context for the terminal Ediacaran biomineralization of animals. Geobiology, 14: 344–363 https://doi.org/10.1111/gbi.12178.
Cui, H., Kaufman, A.J., Xiao, S., Zhou, C., Liu, X.-M., 2017. Was the Ediacaran Shuram Excursion a globally synchronized early diagenetic event? Insights from methane-derived authigenic carbonates in the uppermost Doushantuo Formation, South China. Chemical Geology, 450: 59–80 https://doi.org/10.1016/j.chemgeo.2016.12.010.
Cui, H., Kaufman, A.J., Xiao, S., Zhu, M., Zhou, C., Liu, X.-M., 2015. Redox architecture of an Ediacaran ocean margin: Integrated chemostratigraphic ($\delta^{13}C$–$\delta^{34}S$–$^{87}Sr/^{86}Sr$–Ce/Ce*) correlation of the Doushantuo Formation, South China. Chemical Geology, 405: 48–62 https://doi.org/10.1016/j.chemgeo.2015.04.009.

Cui, H., Xiao, S., Cai, Y., Peek, S., Plummer, R.E., Kaufman, A.J., 2019. Sedimentology and chemostratigraphy of the terminal Ediacaran Dengying Formation at the Gaojiashan section, South China. Geological Magazine, 156: 1924–1948 https://doi.org/10.1017/S0016756819000293.
de Villiers, S., 1999. Seawater strontium and Sr/Ca variability in the Atlantic and Pacific oceans. Earth and Planetary Science Letters, 171(4): 623–634 https://doi.org/10.1016/S0012-821X(99)00174-0.
Delfour, J., 1970. Le Groupe de J'Balah, une nouvelle unite du Bouclier Arabe. Bureau de Recherche Geologique et Minieres Bulletin,(Ser. 2), 4(4): 19–32
Fedonkin, M.A., Gehling, J.G., Grey, K., Narbonne, G.M., Vickers-Rich, P., 2007. The Rise of Animals: Evolution and Diversification of the Kingdom Animalia. John Hopkins University Press, Baltimore, Maryland, USA, 344 pp.
Fike, D.A., Grotzinger, J.P., 2008. A paired sulfate–pyrite $\delta^{34}S$ approach to understanding the evolution of the Ediacaran–Cambrian sulfur cycle. Geochimica et Cosmochimica Acta, 72: 2636–2648 https://doi.org/10.1016/j.gca.2008.03.021.
Goldstein, S.J., Jacobsen, S.B., 1987. The Nd and Sr isotopic systematics of river-water dissolved material: Implications for the sources of Nd and Sr in seawater. Chemical Geology: Isotope Geoscience section, 66(3): 245–272 https://doi.org/10.1016/0168-9622(87)90045-5.
Goldstein, S.L., Hemming, S.R., 2014. Long-lived Isotopic Tracers in Oceanography, Paleoceanography, and Ice-sheet Dynamics. In: Holland, H.D., Turekian, K.K. (Eds.), Treatise on Geochemistry (Second Edition). Elsevier, Oxford, pp. 453–483 https://doi.org/10.1016/B978-0-08-095975-7.00617-3.
Goldstein, S.L., O'Nions, R.K., Hamilton, P.J., 1984. A Sm-Nd isotopic study of atmospheric dusts and particulates from major river systems. Earth and Planetary Science Letters, 70(2): 221–236 https://doi.org/10.1016/0012-821X(84)90007-4.
Grasse, P., Stichel, T., Stumpf, R., Stramma, L., Frank, M., 2012. The distribution of neodymium isotopes and concentrations in the Eastern Equatorial Pacific: Water mass advection versus particle exchange. Earth and Planetary Science Letters, 353–354: 198-207 https://doi.org/10.1016/j.epsl.2012.07.044.
Halverson, G.P., Cox, G.M., Hubert-Théou, L., Schmitz, M., Hagadorn, J.W., Johnson, P., Sansjofre, P., Kunzmann, M., 2013a. A multi-proxy record from a late Neoproterozoic volcano-sedimentary basin, eastern Arabian Shield, Goldschmidt2013 Conference Abstracts.
Halverson, G.P., Cox, G.M., Hubert-Théou, L., Schmitz, M., Hagadorn, J.W., Johnson, P., Sansjofre, P., Kunzmann, M., Schumann, D., 2013b. A multi-proxy geochemical record from a late Neoproterozoic volcano-sedimentary basin, eastern Arabian Shield, McGill Univesity, Canada, unpublished poster.
Halverson, G.P., Dudás, F.Ö., Maloof, A.C., Bowring, S.A., 2007. Evolution of the $^{87}Sr/^{86}Sr$ composition of Neoproterozoic seawater. Palaeogeography, Palaeoclimatology, Palaeoecology, 256(3–4): 103–129 https://doi.org/10.1016/j.palaeo.2007.02.028.
Halverson, G.P., Hoffman, P.F., Schrag, D.P., Maloof, A.C., Rice, A.H.N., 2005. Toward a Neoproterozoic composite carbon-isotope record. Geological Society of America Bulletin, 117(9-10): 1181–1207 https://doi.org/10.1130/b25630.1.
Hamilton, P.J., O'Nions, R.K., Bridgwater, D., Nutman, A., 1983. Sm-Nd studies of Archaean metasediments and metavolcanics from West Greenland and their implications for the

Earth's early history. Earth and Planetary Science Letters, 62(2): 263–272 https://doi.org/10.1016/0012-821X(83)90089-4.
Henjes-Kunst, F., Altherr, R., Baumann, A., 1990. Evolution and composition of the lithospheric mantle underneath the western Arabian peninsula: constraints from Sr-Nd isotope systematics of mantle xenoliths. Contributions to Mineralogy and Petrology, 105(4): 460–472 https://doi.org/10.1007/bf00286833.
Hofmann, A., 2014. 3.3 - Sampling Mantle Heterogeneity through Oceanic Basalts: Isotopes and Trace Elements. In: Holland, H.D., Turekian, K.K. (Eds.), Treatise on Geochemistry (Second Edition) Elsevier, Oxford, pp. 67–101 https://doi.org/10.1016/b0-08-043751-6/02123-x.
Hu, R., Wang, W., Li, S.-Q., Yang, Y.-Z., Chen, F., 2016. Sedimentary Environment of Ediacaran Sequences of South China: Trace Element and Sr-Nd Isotope Constraints. The Journal of Geology, 124(6): 769–789 https://doi.org/10.1086/688668.
Huang, J., Chu, X., Lyons, T.W., Planavsky, N.J., Wen, H., 2013. A new look at saponite formation and its implications for early animal records in the Ediacaran of South China. Geobiology, 11(1): 3–14 https://doi.org/10.1111/gbi.12018.
Ivantsov, A.Y., 2013. New data on Late Vendian problematic fossils from the genus *Harlaniella*. Stratigraphy and Geological Correlation, 21(6): 592–600 https://doi.org/10.1134/s0869593813060051.
Ivantsov, A.Y., Gritsenko, V.P., Konstantinenko, L.I., Zakrevskaya, M.A., 2014a. Revision of the problematic Vendian macrofossil *Beltanelliformis* (=*Beltanelloides*, *Nemiana*). Paleontological Journal, 48(13): 1415–1440 https://doi.org/10.1134/s0031030114130036.
Ivantsov, A.Y., Vickers-Rich, P., Kattan, F., P., T., 2014b. Macrofossils of Late Precambrian of Saudi Arabia, Paleostrat-2014: Annual Assembly of the Paleontological Section of the Moscow Society of Nature Explorers: Program and Theses of Reports, Moscow, Russia, pp. 31–32 (in Russian).
Jacobsen, S.B., Kaufman, A.J., 1999. The Sr, C and O isotopic evolution of Neoproterozoic seawater. Chemical Geology, 161(1–3): 37–57 https://doi.org/10.1016/s0009-2541(99)00080-7.
Jacobsen, S.B., Wasserburg, G.J., 1980. Sm-Nd isotopic evolution of chondrites. Earth and Planetary Science Letters, 50(1): 139–155 https://doi.org/10.1016/0012-821x(80)90125-9.
Johnson, P.R., 2006. Explanatory notes to the map of Proterozoic geology of western Saudi Arabia. . Technical Report, Saudi Geological Survey, SGS-TR-2006 G,1427 H 2006 G: 1-62 + map.
Johnson, P.R., 2014. An expanding Arabian-Nubian Shield geochronologic and isotopic dataset: defining limits and confirming the tectonic setting of a Neoproterozoic accretionary orogen. Open Geology Journal, 8(1): 3–33 https://doi.org/10.2174/1874262901408010003.
Johnson, P.R., Andresen, A., Collins, A.S., Fowler, A.R., Fritz, H., Ghebreab, W., Kusky, T., Stern, R.J., 2011. Late Cryogenian–Ediacaran history of the Arabian–Nubian Shield: A review of depositional, plutonic, structural, and tectonic events in the closing stages of the northern East African Orogen. Journal of African Earth Sciences, 61(3): 167–232 https://doi.org/10.1016/j.jafrearsci.2011.07.003.
Kaufman, A.J., Jacobsen, S.B., Knoll, A.H., 1993. The Vendian record of Sr and C isotopic variations in seawater: implications for tectonics and paleoclimate. Earth and Planetary Science Letters, 120(3): 409–430 https://doi.org/10.1016/0012-821x(93)90254-7.

Knoll, A.H., 2000. Learning to tell Neoproterozoic time. Precambrian Research, 100(1–3): 3–20 https://doi.org/10.1016/s0301-9268(99)00067-4.

Kozdrój, W., Kennedy, A.K., Johnson, P.R., Ziółkowska-Kozdrój, M., Kadi, K., 2018. Geochronology in the southern Midyan terrane: a review of constraints on the timing of magmatic pulses and tectonic evolution in a northwestern part of the Arabian Shield. International Geology Review, 60(10): 1290–1319 https://doi.org/10.1080/00206814.2017.1385425.

Kuznetsov, A., Semikhatov, M., Gorokhov, I., 2012. The Sr isotope composition of the world ocean, marginal and inland seas: Implications for the Sr isotope stratigraphy. Stratigraphy and Geological Correlation, 20(6): 501–515 https://doi.org/10.1134/S0869593812060044.

Lacan, F., Tachikawa, K., Jeandel, C., 2012. Neodymium isotopic composition of the oceans: A compilation of seawater data. Chemical Geology, 300-301(0): 177–184 https://doi.org/10.1016/j.chemgeo.2012.01.019.

Le Guerroué, E., Allen, P.A., Cozzi, A., Etienne, J.L., Fanning, M., 2006. 50 Myr recovery from the largest negative $\delta^{13}C$ excursion in the Ediacaran ocean. Terra Nova, 18(2): 147–153 https://doi.org/10.1111/j.1365-3121.2006.00674.x.

Liu, C., Wang, Z., Raub, T.D., 2013. Geochemical constraints on the origin of Marinoan cap dolostones from Nuccaleena Formation, South Australia. Chemical Geology, 351(0): 95–104 https://doi.org/10.1016/j.chemgeo.2013.05.012.

Liu, C., Wang, Z., Raub, T.D., Macdonald, F.A., Evans, D.A., 2014. Neoproterozoic cap-dolostone deposition in stratified glacial meltwater plume. Earth and Planetary Science Letters, 404: 22–32 https://doi.org/10.1016/j.epsl.2014.06.039.

Liu, X.-M., Kah, L.C., Knoll, A.H., Cui, H., Kaufman, A.J., Shahar, A., Hazen, R.M., 2016. Tracing Earth's O_2 evolution using Zn/Fe ratios in marine carbonates. Geochemical Perspectives Letters, 2: 24–34 https://doi.org/10.7185/geochemlet.1603.

Lugmair, G.W., Marti, K., 1978. Lunar initial $^{143}Nd/^{144}Nd$: Differential evolution of the lunar crust and mantle. Earth and Planetary Science Letters, 39(3): 349–357 https://doi.org/10.1016/0012-821X(78)90021-3.

Macdonald, F.A., Strauss, J.V., Sperling, E.A., Halverson, G.P., Narbonne, G.M., Johnston, D.T., Kunzmann, M., Schrag, D.P., Higgins, J.A., 2013. The stratigraphic relationship between the Shuram carbon isotope excursion, the oxygenation of Neoproterozoic oceans, and the first appearance of the Ediacara biota and bilaterian trace fossils in northwestern Canada. Chemical Geology, 362: 250–272 https://doi.org/10.1016/j.chemgeo.2013.05.032.

McArthur, J.M., Howarth, R.J., Shields, G.A., 2012. Strontium Isotope Stratigraphy. In: Gradstein, F.M., Ogg, J.G., Schmitz, M.D., Ogg, G.M. (Eds.), The Geologic Time Scale. Elsevier, Boston, pp. 127–144 https://doi.org/10.1016/b978-0-444-59425-9.00007-x.

Meija, J., Coplen, T.B., Berglund, M., Brand, W.A., De Bièvre, P., Gröning, M., Holden, N.E., Irrgeher, J., Loss, R.D., Walczyk, T., 2016. Atomic weights of the elements 2013 (IUPAC Technical Report). Pure and Applied Chemistry, 88(3): 265-291 https://doi.org/10.1515/pac-2015-0305.

Melezhik, V.A., Pokrovsky, B.G., Fallick, A.E., Kuznetsov, A.B., Bujakaite, M.I., 2009. Constraints on $^{87}Sr/^{86}Sr$ of Late Ediacaran seawater: insight from Siberian high-Sr limestones. Journal of the Geological Society, 166(1): 183–191 https://doi.org/10.1144/0016-76492007-171.

Miller, N., Johnson, P.R., Stern, R.J., 2008. Marine versus non-marine environments for the Jibalah Group, NW Arabian Shield: A sedimentologic and geochemical survey and report of possible metazoa in the Dhaiqa Formation. Arabian Journal for Science and Engineering, 33(1): 55–78

Moghazi, A.-K.M., Ali, K.A., Wilde, S.A., Zhou, Q., Andersen, T., Andresen, A., Abu El-Enen, M.M., Stern, R.J., 2012. Geochemistry, geochronology, and Sr–Nd isotopes of the Late Neoproterozoic Wadi Kid volcano-sedimentary rocks, Southern Sinai, Egypt: Implications for tectonic setting and crustal evolution. Lithos, 154: 147–165 https://doi.org/10.1016/j.lithos.2012.07.003.

Moufti, M., Moghazi, A., Ali, K., 2012. Geochemistry and Sr–Nd–Pb isotopic composition of the Harrat Al-Madinah Volcanic Field, Saudi Arabia. Gondwana Research, 21(2): 670–689 https://doi.org/10.1016/j.gr.2011.06.003.

Narbonne, G.M., 2005. The Ediacara Biota: Neoproterozoic origin of animals and their ecosystems. Annual Review of Earth and Planetary Sciences, 33: 421–442 https://doi.org/10.1146/annurev.earth.33.092203.122519.

Narbonne, G.M., Kaufman, A.J., Knoll, A.H., 1994. Integrated chemostratigraphy and biostratigraphy of the Windermere Supergroup, northwestern Canada: Implications for Neoproterozoic correlations and the early evolution of animals. Geological Society of America Bulletin, 106(10): 1281–1292 https://doi.org/10.1130/0016-7606(1994)106<1281:icabot>2.3.co;2.

Nettle, D., Halverson, G.P., Cox, G.M., Collins, A.S., Schmitz, M., Gehling, J., Johnson, P.R., Kadi, K., 2014. A middle–late Ediacaran volcano - sedimentary record from the eastern Arabian - Nubian shield. Terra Nova, 26(2): 120-129 https://doi.org/10.1111/ter.12077.

Ojiambo, S.B., Lyons, W.B., Welch, K.A., Poreda, R.J., Johannesson, K.H., 2003. Strontium isotopes and rare earth elements as tracers of groundwater–lake water interactions, Lake Naivasha, Kenya. Applied Geochemistry, 18(11): 1789–1805 https://doi.org/10.1016/S0883-2927(03)00104-5.

Puchtel, I.S., Blichert-Toft, J., Touboul, M., Walker, R.J., Byerly, G.R., Nisbet, E.G., Anhaeusser, C.R., 2013. Insights into early Earth from Barberton komatiites: Evidence from lithophile isotope and trace element systematics. Geochimica et Cosmochimica Acta, 108: 63–90 https://doi.org/10.1016/j.gca.2013.01.016.

Rad, S.D., Allègre, C.J., Louvat, P., 2007. Hidden erosion on volcanic islands. Earth and Planetary Science Letters, 262(1): 109–124 https://doi.org/10.1016/j.epsl.2007.07.019.

Ries, J.B., Fike, D.A., Pratt, L.M., Lyons, T.W., Grotzinger, J.P., 2009. Superheavy pyrite ($\delta^{34}S_{pyr} > \delta^{34}S_{CAS}$) in the terminal Proterozoic Nama Group, southern Namibia: A consequence of low seawater sulfate at the dawn of animal life. Geology, 37(8): 743–746 https://doi.org/10.1130/g25775a.1.

Robinson, F.A., Foden, J.D., Collins, A.S., 2015. Geochemical and isotopic constraints on island arc, synorogenic, post-orogenic and anorogenic granitoids in the Arabian Shield, Saudi Arabia. Lithos, 220–223: 97–115 https://doi.org/10.1016/j.lithos.2015.01.021.

Rudnick, R.L., Gao, S., 2014. 4.1 - Composition of the Continental Crust. In: Holland, H.D., Turekian, K.K. (Eds.), Treatise on Geochemistry (Second Edition). Elsevier, Oxford, pp. 1–51 https://doi.org/10.1016/B978-0-08-095975-7.00301-6.

Sawaki, Y., Ohno, T., Tahata, M., Komiya, T., Hirata, T., Maruyama, S., Windley, B.F., Han, J., Shu, D., Li, Y., 2010. The Ediacaran radiogenic Sr isotope excursion in the Doushantuo

Formation in the Three Gorges area, South China. Precambrian Research, 176(1–4): 46–64 https://doi.org/10.1016/j.precamres.2009.10.006.

Stern, R.J., Johnson, P.R., Ali, K.A., Mukherjee, S.K., 2011. Evidence for Early and Mid-Cryogenian glaciation in the Northern Arabian–Nubian Shield (Egypt, Sudan, and western Arabia). Geological Society, London, Memoirs, 36(1): 277-284 https://doi.org/10.1144/M36.22.

Tachikawa, K., Arsouze, T., Bayon, G., Bory, A., Colin, C., Dutay, J.-C., Frank, N., Giraud, X., Gourlan, A.T., Jeandel, C., Lacan, F., Meynadier, L., Montagna, P., Piotrowski, A.M., Plancherel, Y., Pucéat, E., Roy-Barman, M., Waelbroeck, C., 2017. The large-scale evolution of neodymium isotopic composition in the global modern and Holocene ocean revealed from seawater and archive data. Chemical Geology, 457: 131–148 https://doi.org/10.1016/j.chemgeo.2017.03.018.

Tachikawa, K., Athias, V., Jeandel, C., 2003. Neodymium budget in the modern ocean and paleo - oceanographic implications. Journal of Geophysical Research: Oceans, 108(C8): 3254 https://doi.org/10.1029/1999JC000285.

Taylor, S.R., McLennan, S.M., 1985. The Continental Crust: Its Composition and Evolution. Blackwell Scientific Publications, Palo Alto, California, USA.

Vickers-Rich, P., Ivantsov, A., Kattan, F.H., Johnson, P.R., Al Qubsani, A., Kasghari, W., Leonov, M., Rich, T., Linnemann, U., Hoffman, M., Trusler, P., Smith, J., Yazedi, A., Rich, B., Al Gani, S.M., Shamari, A., Al Barakati, A., Al Kaff, M.H., 2013. In Search of the Kingdom's Ediacarans: The First Genuine Metazoans (Mcaroscopic Body and Trace Fossils) from the Neoproterozoic Jibalah group (Vendian/Ediacaran) on the Arabian Shield, Saudi Geological Survey Technical Report, SGS–TR–2013–5: 1–21.

Vickers-Rich, P., Kozdroj, W., Kattan, F.H., Leonov, M., Ivantsov, A., Johnson, P.R., Linnemann, U., Hofmann, M., Al Garni, S.M., Al Qubsani, A., Shamari, A., Al Barakati, A., Al Kaff, M.H., Ziolkowska-Kozdroj, M., Rich, T., Trusler, P., Rich, B., 2010. Reconnaissance for an Ediacaran Fauna, Kingdom of Saudi Arabia, Saudi Geological Survey Technical Report, SGS–TR–2010–8: 1–42.

Wei, G.-Y., Hood, A.v.S., Chen, X., Li, D., Wei, W., Wen, B., Gong, Z., Yang, T., Zhang, Z.-F., Ling, H.-F., 2019a. Ca and Sr isotope constraints on the formation of the Marinoan cap dolostones. Earth and Planetary Science Letters, 511: 202–212 https://doi.org/10.1016/j.epsl.2019.01.024.

Wei, G.-Y., Ling, H.-F., Shields, G.A., Chen, T., Lechte, M., Chen, X., Qiu, C., Lei, H., Zhu, M., 2019b. Long-term evolution of terrestrial inputs from the Ediacaran to early Cambrian: Clues from Nd isotopes in shallow-marine carbonates, South China. Palaeogeography, Palaeoclimatology, Palaeoecology, 535: 109367 https://doi.org/10.1016/j.palaeo.2019.109367.

White, W.M., 2013. Geochemistry. Wiley-Blackwell, Hoboken, New Jersey, USA.

Xiao, S., Narbonne, G.M., Zhou, C., Laflamme, M., Grazhdankin, D.V., Moczydłowska-Vidal, M., Cui, H., 2016. Toward an Ediacaran time scale: Problems, protocols, and prospects. Episodes, 39: 540–555 https://doi.org/10.18814/epiiugs/2016/v39i4/103886.

Yang, J., Tao, X., Xue, Y., 1997. Nd isotopic variations of Chinese seawater during Neoproterozoic through Cambrian. Chemical geology, 135(1): 127–137 https://doi.org/10.1016/S0009-2541(95)00152-2.

Zhu, M., Gehling, J.G., Xiao, S., Zhao, Y., Droser, M.L., 2008. Eight-armed Ediacara fossil preserved in contrasting taphonomic windows from China and Australia. Geology, 36(11): 867-870 https://doi.org/10.1130/g25203a.1.